Article

Developmental Cell

Global Analysis of mRNA, Translation, and Protein Localization: Local Translation Is a Key Regulator of Cell Protrusions

Highlights

- Local translation is a key regulator of protein localization to cell protrusions
- Localization of mRNAs alone, however, does not determine local protein expression
- Specific UTR elements and RBPs are associated with local translation in protrusions
- Inhibition of local translation destabilizes protrusions

Authors

Faraz K. Mardakheh, Angela Paul, Sandra Kümper, ..., Afshan Mccarthy, Yinyin Yuan, Christopher J. Marshall

Correspondence

mardakheh@icr.ac.uk

In Brief

Establishment of front-back cell polarity is the first step in any form of active cell migration. Mardakheh et al. show that in mesenchymal-like cells, front-back asymmetry at the proteome level is maintained by differential local synthesis of cellular proteins.

Mardakheh et al., 2015, Developmental Cell *35*, 344–357
November 9, 2015
http://dx.doi.org/10.1016/j.devcel.2015.10.005

CellPress

CellPress

Developmental Cell
Article

Global Analysis of mRNA, Translation, and Protein Localization: Local Translation Is a Key Regulator of Cell Protrusions

Faraz K. Mardakheh,[1,*] Angela Paul,[1] Sandra Kümper,[1] Amine Sadok,[1] Hugh Paterson,[1] Afshan Mccarthy,[1] Yinyin Yuan,[2] and Christopher J. Marshall[1,3]

[1]Division of Cancer Biology, Institute of Cancer Research, 237 Fulham Road, London SW3 6JB, UK
[2]Division of Molecular Pathology, Institute of Cancer Research, 237 Fulham Road, London SW3 6JB, UK
[3]Deceased
*Correspondence: mardakheh@icr.ac.uk
http://dx.doi.org/10.1016/j.devcel.2015.10.005

SUMMARY

Polarization of cells into a protrusive front and a retracting cell body is the hallmark of mesenchymal-like cell migration. Many mRNAs are localized to protrusions, but it is unclear to what degree mRNA localization contributes toward protrusion formation. We performed global quantitative analysis of the distributions of mRNAs, proteins, and translation rates between protrusions and the cell body by RNA sequencing (RNA-seq) and quantitative proteomics. Our results reveal local translation as a key determinant of protein localization to protrusions. Accordingly, inhibition of local translation destabilizes protrusions and inhibits mesenchymal-like morphology. Interestingly, many mRNAs localized to protrusions are translationally repressed. Specific *cis*-regulatory elements within mRNA UTRs define whether mRNAs are locally translated or repressed. Finally, RNAi screening of RNA-binding proteins (RBPs) enriched in protrusions revealed *trans*-regulators of localized translation that are functionally important for protrusions. We propose that by deciphering the localized mRNA UTR code, these proteins regulate protrusion stability and mesenchymal-like morphology.

INTRODUCTION

A pre-requisite of cell migration is the establishment of front-back cell polarity (Etienne-Manneville, 2008). In mesenchymal-like cells, the front is protrusive, characterized by a network of newly generated actin filaments, while the back is retractile, pulling up the body of the cell toward the direction of migration (Sahai and Marshall, 2003). This asymmetry in morphology and function between the front and back has been shown to be associated with differential localization of proteins to protrusions and the cell body, many of which are associated with actin cytoskeleton (Small and Resch, 2005). Actin is polymerized at the leading edge by actin nucleating factors such as the ARP2/3 complex and formins. Other actin binding proteins, such as capping, bundling, and severing proteins, further regulate actin cytoskeleton organization by affecting the dynamics of existing filaments. In the cell body, myosin II association with actin filaments generates contractile force, which is crucial for adhesion maturation and tail retraction (Ridley, 2011). The signaling that initiates protrusions is relayed by a wide variety of signaling molecules. These include lipid second messengers such as phosphatidylinositol-phosphates, as well as members of the Rho family of small GTPases, in particular RHO, RAC, and CDC42, which trigger and coordinate front-back polarization and spatial organization of the actin cytoskeleton (Cain and Ridley, 2009; Ridley, 2011).

While much is known about the mechanisms that trigger protrusion formation, little is known about how front-back cell asymmetry is maintained in migrating cells. In addition to differential distribution of proteins, mRNAs are also differentially distributed between the front and back of the cells (Condeelis and Singer, 2005; Mili et al., 2008; Mingle et al., 2005). Cellular mRNAs are known to be transported via microtubule or actin filaments (St Johnston, 2005). Once localized, mRNAs could be subject to local translation (Halstead et al., 2015; Hüttelmaier et al., 2005; Yasuda et al., 2013), which would result in increased local concentration of their corresponding proteins. Importantly, the mechanisms that regulate mRNA targeting and translation in protrusions are poorly defined. Moreover, to what extent mRNA localization and local translation define front-back asymmetry and protrusion formation remains to be determined.

Here, we assessed how mRNA localization and local translation contributes toward front-back asymmetry at the proteome level. We used a proteomics approach, quantifying the distribution of cellular proteins between protrusions and the cell body by stable isotope labeling of amino acids in culture (SILAC) (Ong et al., 2002). Using a pulse labeling variation of the SILAC strategy known as pulsed-SILAC (Selbach et al., 2008), we also determined the relative translation rates of proteins between protrusions and the cell body. Finally, we quantified the relative distribution of mRNAs between protrusions and the cell body by RNA sequencing (RNA-seq). Comparison of relative protein distributions with mRNA distributions showed little correlation between the two, suggesting that mRNA localization alone does not determine protein localization to protrusions. However, relative translation rates between protrusions and the cell body exhibited a significant correlation with protein distributions,

suggesting that localized translation is a significant determinant of front-back cell asymmetry. Accordingly, we show that local protein translation in protrusion is crucial for stabilizing protrusions and maintaining a mesenchymal-like polarized morphology. Analysis of mRNA UTR elements revealed several conserved motifs that were enriched in locally translated mRNAs, suggesting that their absence or presence can control local translation rates. To reveal *trans*-regulators of local translation that were functionally important for protrusions, we screened RBP categories enriched in protrusions by RNAi. We found several RBPs that significantly regulated protrusions and mesenchymal-like migration. These included many known but also a number of novel regulators of mRNA localization and local translation including the exosome core complex (Lykke-Andersen et al., 2009). We demonstrate that the exosome core, but not its catalytic subunits, is highly enriched in protrusions and is essential for protrusion stability but not initiation. Our work establishes local translation as a key regulator of asymmetric distribution of the proteome between protrusions and the cell body, describes *cis*-regulatory UTR motifs that are associated with localized translation in protrusions, and highlights *trans*-acting RBPs that are involved in regulation of protrusions and mesenchymal-like migration.

RESULTS

Local Translation Is a Key Determinant of Protein Localization to Protrusions

To study cell protrusions, we used a micro-porous filter-based method to separate protrusions from cell bodies of highly protrusive MDA-MB231 breast cancer cells (Shankar et al., 2010; Wang et al., 2007). In this method, cells are seeded on top of collagen-I-coated 3-μm transwell filters to enable protrusions to form but to prevent the cell bodies from passing through due to the size of the pores, resulting in separation of protrusions and the cell bodies on opposite sides of the filter (Figures 1A and 1B). As expected (Sanz-Moreno et al., 2008), these protrusions are dependent on Rho-GTPases RAC1 and CDC42 (Figure 1C) and are enriched in known protein markers of protrusive fronts such as VASP (Rottner et al., 1999), PAX (Nobes and Hall, 1995), ZYX (Crawford et al., 1992), as well as F-actin (Figures 1D and 1E). In terms of spatial and temporal dynamics, protrusion formation through transwell pores seems to be a good mimic of protrusion formation in 3D matrices, where cells have to similarly protrude through matrix pores and holes. In fact, the transwell pore size of 3 μm is comparable to the average pore size of pepsinized collagen-I 3D matrices (Wolf et al., 2009), and average diameters of protrusions extended through these transwell pores (~3 μm wide, ~10–15 μm long, dictated by pore size diameters) are comparable to the diameters of protrusions in 3D collagen-I (Figures 1F and 1G). In addition, the temporal dynamics of protrusions extended through transwell pores are similar to those extended in 3D collagen-I, with protrusions remaining stable for various lengths of time, from minutes to several hours, with a median length of over 2 hr (Figures 1H and 1I; Movies S1 and S2).

Using the transwell-based fractionation method, we first determined the distribution of cellular proteins between protrusions and the cell body by quantitative proteomics (Figure 2A), revealing the relative distribution of 3,334 proteins from two reciprocally labeled SILAC experiments (Data S1A). Overall, the proteome exhibited a normal-like distribution between protrusions and the cell body, with different proteins being enriched or depleted in protrusions to various levels (Figure 2B). Annotation enrichment analysis (Cox and Mann, 2012) revealed multiple protein categories that were significantly enriched or depleted in protrusions (Data S1B). As expected, the majority of the protrusion-enriched proteins belonged to known actin-associated categories (Data S1B). These included upstream signaling regulators of protrusion formation, actin polymerizing factors such as the ARP2/3 complex and its upstream regulator WAVE2, as well as other actin binding and adhesion molecules such as VASP, ENAH, and PXN (Data S1B). On the other hand, the majority of cell body-enriched proteins were those of nucleus, ER, mitochondria, and other organelles (Data S1B). Interestingly, several categories of RNA-binding proteins (RBPs), translation factors, and protein folding chaperones were enriched in protrusions (Data S1B), indicating that a significant level of localized protein synthesis may occur in protrusions.

In order to determine to what level mRNA localization contributes toward protein localization in protrusions, we quantified the distribution of cellular mRNAs between protrusions and the cell body by RNA-seq (Figure S1A; Data S1C). Similar to the proteome distribution, RNA-seq revealed a normal-like distribution, with different mRNAs being enriched or depleted to different degrees between protrusions and the cell body (Figure 2C). Surprisingly, no correlation was detected between mRNA and protein distributions (Figure 2D), suggesting that mRNA localization alone is not a significant predictor of protein localization to protrusions. As a validation of our method, we compared our RNA-seq dataset against a previously published microarray-based protrusion/cell body mRNA localization study in mouse NIH/3T3 fibroblasts (Mili et al., 2008). There was a very strong overlap between the two datasets (Figure S1B), suggesting that RNA localization at the global level is likely to be conserved across species and cell types, despite a lack of correlation with protein distributions.

Next, we assessed whether local translation contributes toward protein localization to protrusions. We quantified relative translation rates of proteins between protrusions and the cell body during a 2 hr transwell protrusion formation assay by utilizing a variation of the SILAC method called pulsed SILAC (pSILAC) (Selbach et al., 2008) (Figure 2E). We determined the relative translation rates of 1,150 proteins between protrusions and the cell body (Data S1D). The lower coverage compared to the proteome analysis was expected, as the medium and heavy peptides that are used for pSILAC quantification are significantly low in abundance after a short 2 hr labeling. Nevertheless, widespread localized translation was evident, with many cellular proteins displaying higher translation in protrusions than the cell body and vice-versa (Figure 2F). Moreover, we observed a significant correlation between relative translation rate and protein localization (Figure 2G). Pearson's correlation coefficient between protein and translation rate distributions was 0.30. The actual correlation is likely to be even higher, considering that the Pearson's correlation coefficients between the two SILAC and pSILAC replicates were 0.72 and 0.66, respectively, presumably due to the inherent errors of the mass

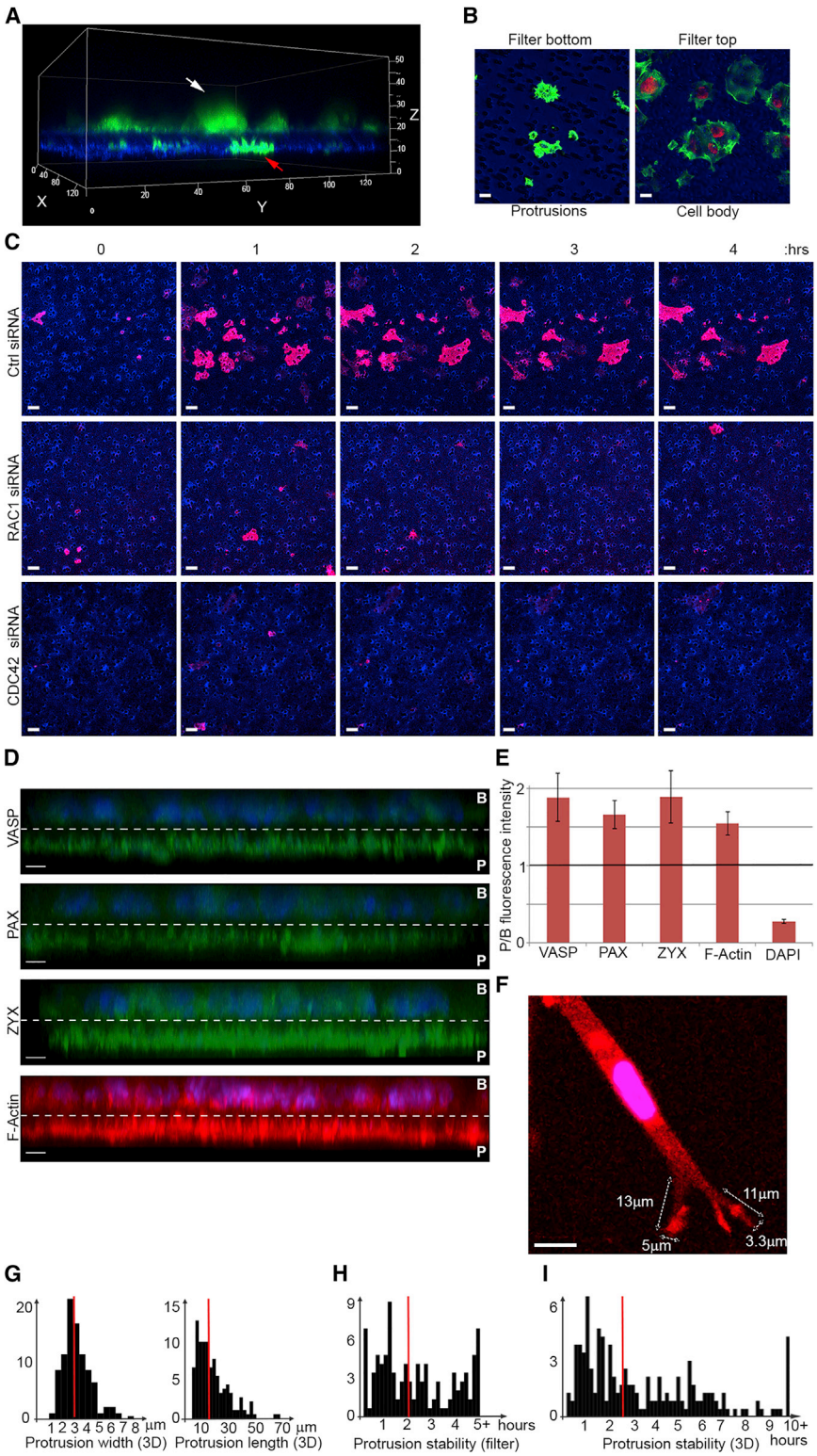

Figure 1. Filter-Based Analysis of Protrusions in MDA-MB231 Cells

(A) Confocal 3D rendering of MDA-MB231 cells forming protrusions through 3-μm transwell filters. Cells were stained with CellTracker-CMFDA (green) 24 hr prior to seeding. The collagen coated filter was stained prior to seeding by CellTrace Far Red DDAO-SE (blue). White arrow, cell body; red arrow, protrusions. Axes scales are in μm.

(B) Transwell separated protrusions are actin-rich, but lack a nucleus. MDA-MB231 cells protruding through 3-μm transwell filters were fixed and stained with phalloidin-Alexa Fluor-488 (green) and Hoechst (red). Confocal images were taken from the top (right image) and bottom (left image) of the filter. The filter was visualized by transmitted light (blue). Scale bar, 10 μm.

(C) Formation of protrusions is dependent on RAC1 and CDC42. Control, RAC1, or CDC42 siRNA transfected MDA-MB231 mKate-CAAX cells (red) were seeded on collagen-coated 3-μm transwell filters and time-lapsed as they formed protrusions through the pores. Confocal images were taken from the bottom of the filter. Collagen coated filters were stained by CellTrace Far Red DDAO-SE (blue) prior to seeding. Scale bar, 10 μm.

(D) Protrusions formed through transwell filters are enriched in VASP, PXN, ZYX, and F-actin. Cross-section side views of confocal 3D renderings of MDA-MB231 cells protruding through 3-μm transwell filters. Cells were fixed and immunostained with antibodies against indicated markers (green), or phalloidin for F-actin staining (red). DAPI was used for nuclear staining (blue). Dashed line marks the position of the filter. Protrusions are marked as (P) and the cell-bodies are marked as (B). Scale bar, 10 μm.

(E) Quantification of the protrusion (P)/cell body (B) fluorescent intensities for indicated markers from (D). At least three independent tiled scans, each formed from nine fields of view, were used. All error bars are SD.

(F) Protrusion diameters of MDA-MB231 cells in 3D pepsinized collagen-I are comparable to transwell protrusion diameters. MDA-MB231 mKate-CAAX cells (red) were seeded on 3D collagen-I gels and imaged 2–4 hr after seeding by confocal microscopy. Scale bar, 10 μm.

(G) Protrusion width and length measurements from 92 cells (as in F) are displayed as histograms. A total of 172 individual protrusions were measured. Average protrusion width in 3D collagen-I is 3.1 μm (red line). Average protrusion length in 3D collagen-I is 16.5 μm (red line).

(H) Transwell protrusions are stable for a variety of time lengths, with a median stability of 2 hr and 5 min. The stability of protrusions was assessed from nine time-lapse movies of protrusion formation through 3-μm transwell filters (see also Movie S1). A total of 136 protrusions from 85 cells were timed over a 5-hr period, and the results are displayed as a histogram. Red line marks the median stability (125 min).

(I) 3D protrusions are stable for a variety of time-lengths, with a median stability of 2 hr and 42 min. The stability of protrusions was assessed from four time-lapse movies of protrusion formation in 3D collagen-I (see also Movie S2). A total of 200 protrusions from 99 cells were timed over a 10-hr period. The results are displayed as a histogram. Red line marks the median stability (162 min).

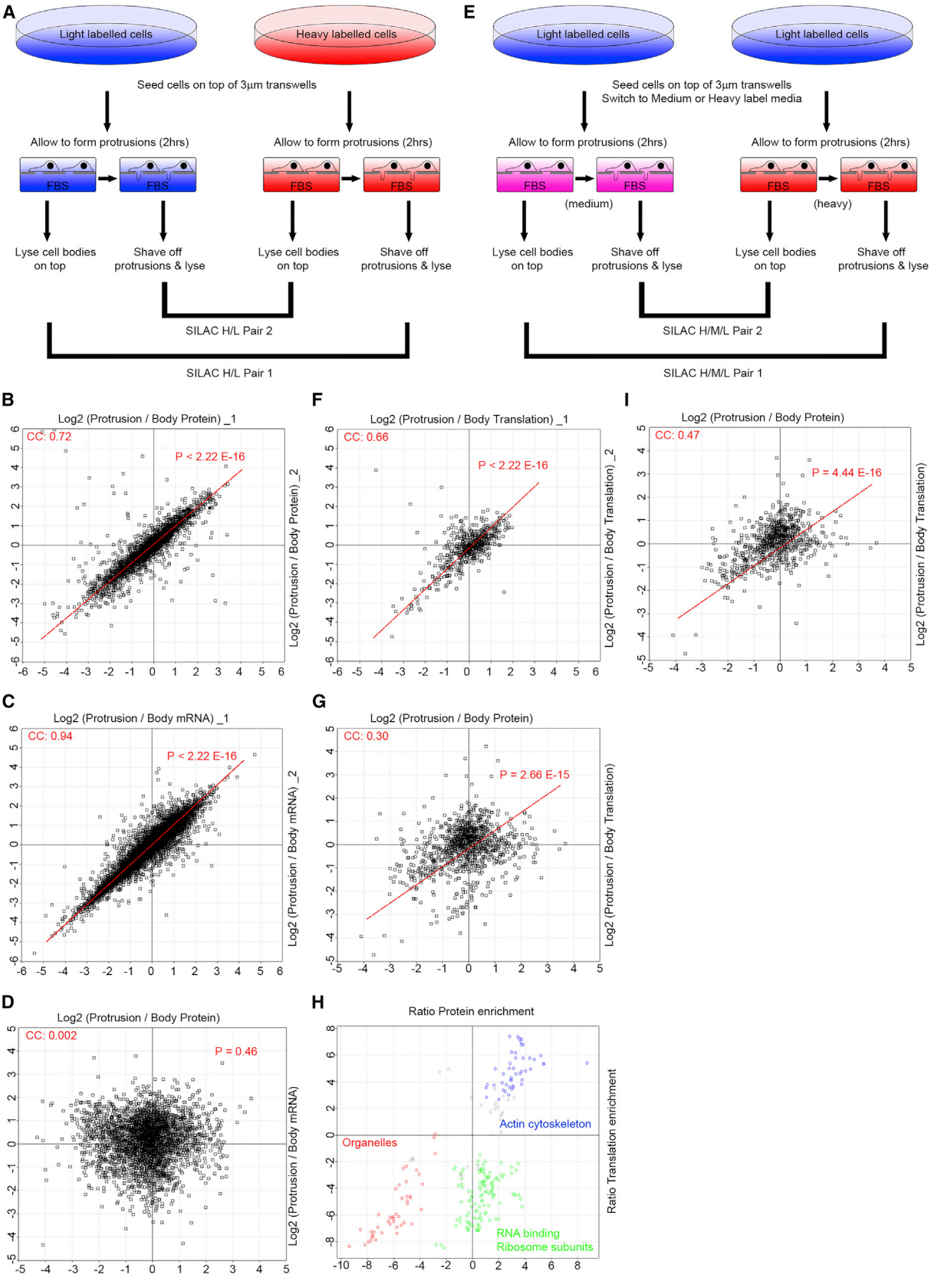

(legend on next page)

spectrometry-based measurements (Figures 2B and 2F). These results demonstrate that localized translation is a key determinant of a significant degree of protein localization to protrusions.

Ribosomes and RNA-Binding Proteins Are Not Locally Translated but Are Transported to Protrusions

We next investigated if the contribution of local translation toward protein localization was uniform across all protein categories or whether certain categories of proteins were more reliant on local translation than others for their localization. We performed a 2D annotation enrichment analysis (Cox and Mann, 2012) to determine which categories of proteins show a positive correlation between their protein enrichment levels and their relative translation rates as opposed to those that exhibit a negative correlation (Data S1E). All actin-associated protrusion-enriched categories showed a strong positive correlation, having both high protrusion protein levels and high protrusion translation levels (Figure 2H). These categories included ARP2/3 complex subunits, adhesion-related proteins, ezrin, filamins, alpha-actinin, and other actin-binding protrusion proteins such as actin capping and LIM domain proteins (Data S1E). Most organelle-associated protein categories depleted in protrusions also showed a positive correlation, exhibiting both low protrusion protein and low protrusion translation levels (Figure 2H). Collectively, these results suggest that the localization of these protein categories is likely to be determined by their localized translation, either in protrusions or at the cell body. In contrast, RNA-binding and ribosomal protein categories exhibited a negative correlation, having significantly lower protrusion translation rates compared to their protrusion protein levels (Figure 2H). In fact, removal of ribosomal and RNA-binding proteins from our datasets resulted in a significant increase in the overall correlation from 0.30 to 0.47 (Figure 2I). These results suggest that while the localization of most protein categories, including all actin-associated protrusion proteins, can be explained by the differences in their localized translation rates, RNA-binding and ribosomal proteins do not follow this rule, indicating that these proteins are likely to be transported to protrusions instead.

Local Translation Is Needed for Protrusion Stability

Our pSILAC data suggest a significant role for local translation in regulation of the asymmetry between protrusions and the cell body at the proteome level. Thus, we predicted that inhibition of local translation in protrusion should inhibit protrusions. We first confirmed the occurrence of localized translation in protrusions by visualizing nascent protein synthesis in protrusion and cell body fractions, using puromycinylation tagging of newly synthesized proteins (Schmidt et al., 2009). Puromycinylation analysis of protrusion and cell body fractions confirmed that protein translation was widespread in protrusions, with overall levels comparable to that of the cell body (Figure 3A). High levels of translation in protrusions could also be revealed by immunofluorescence staining of transwell protruding cells using anti-puromycin staining following puromycinylation (Figure S2A).

Next, we tested whether protein translation was needed for protrusion formation. Treatment of MDA-MB231 cells with cycloheximide-abrogated protein translation (Figures S2A and S2B). Temporal analysis of protrusion formation revealed that MDA-MB231 cells still initiated protrusions in presence of cycloheximide, but these protrusions were unstable and retracted back (Figures 3B and 3C; Movie S3), suggesting that translation acts to stabilize protrusions rather than to initiate them. Cycloheximide treatment also destabilized protrusions in a 3D collagen-I matrix, resulting in conversion of the cells from a polarized mesenchymal-like morphology to round (Figures 3D and 3E; Movie S4). The rounding observed with cycloheximide treatment was not due to apoptosis (Figure S2C), suggesting that protein translation is needed for protrusion stability.

To show that it is localized translation that is needed for protrusion stability, we devised a strategy to inhibit translation specifically in protrusions. We used emetine, an irreversible inhibitor of

Figure 2. Localized Translation, but Not mRNA Targeting, Significantly Contributes toward the Proteome Asymmetry between Protrusions and the Cell Body

(A) Schematic representation of SILAC protrusion proteomics analysis; the H/L ratios are the measures of protrusion/body protein distributions.

(B) Proteome distribution between protrusions and the cell body. Log2 SILAC ratios from reciprocal SILAC mixtures of protrusion and cell body fractions (Data S1A) were plotted against each other. CC, Pearson's correlation coefficient between the two pairs. P value of the correlation is displayed on the graph.

(C) Messenger-RNA distributions between protrusions and the cell body. Log2 of protrusion/cell body FPKM ratios from two replicate experiments (Data S1C) were plotted against each other. CC, Pearson's correlation coefficient between the two replicates. P value of the correlation is displayed on the graph.

(D) Protein distributions between protrusions and the cell body do not correlate with mRNA distributions. Averaged Log2 of protrusion/cell body protein ratios were plotted against averaged Log2 of Protrusion/Cell body mRNA ratios. CC = Pearson's correlation coefficient. P-value of the correlation is displayed on the graph.

(E) Schematic representation of pSILAC protrusion proteomics analysis. H/M ratios for each protein are the measures of protrusion/body translation rates.

(F) Translation rate distributions between protrusions and the cell body. Log2 of H/M SILAC ratios from reciprocal pSILAC mixtures of protrusion and cell body fractions (Data S1D) were plotted against each other. CC, Pearson's correlation coefficient between the two pairs. P value of the correlation is displayed on the graph.

(G) Protein distributions between protrusions and the cell body significantly correlate with translation rate distributions. Averaged Log2 of protrusion/cell body protein ratios from the two reciprocal SILAC pairs were plotted against averaged Log2 of protrusion/cell body pSILAC ratios. CC, Pearson's correlation coefficient. P value of the correlation is displayed on the graph.

(H) RNA-binding proteins and ribosomal components are enriched but not locally synthesized in protrusions. The 2D-annotation enrichment analysis data from Data S1E was plotted with each data point representing a protein category. Most protein categories exhibit a correlative regulation of their protein distributions and relative translation rates, for example all protrusion-enriched actin-related categories (blue), and all protrusion-depleted organelle-related categories (red), but an anti-correlative behavior is observed for RNA-binding and ribosomal protein categories (green), with their relative translation rates significantly lower than their relative protein amounts.

(I) Removal of RNA-binding and ribosomal protein categories from (G) significantly increases the correlation between protein distributions and translation rates from 0.30 to 0.47. CC, Pearson's correlation coefficient. P value of the correlation is displayed on the graph.

See also Figure S1.

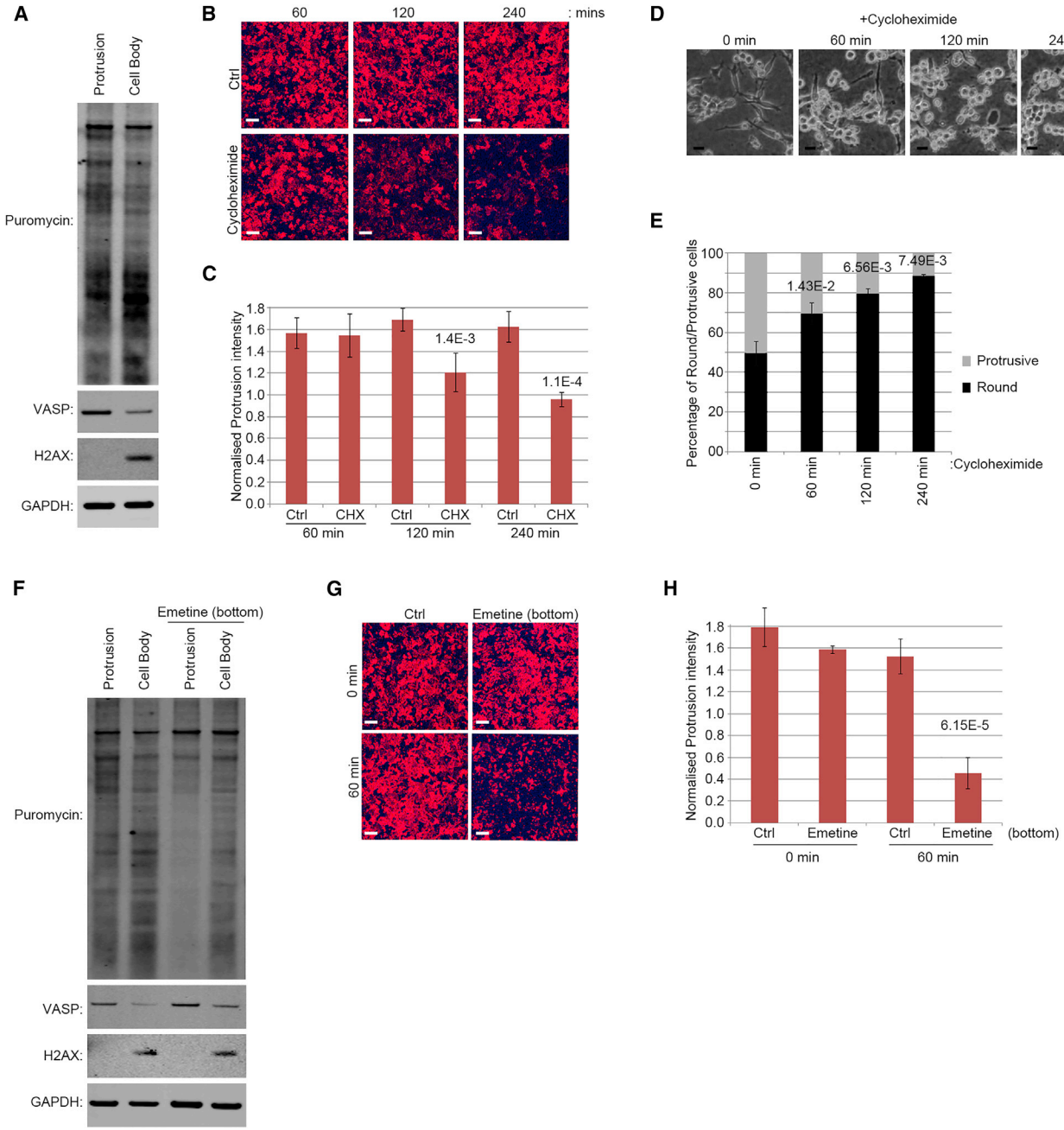

Figure 3. Local Translation Is Needed for Protrusion Stabilization

(A) Widespread translation occurs in protrusions. MDA-MB231 cells seeded on 3-μm transwells for 2 hr were treated with Puromycin (10 μg/ml) for 10 min to label nascent proteins. Equal amounts of isolated protrusion and cell body fractions were then resolved by SDS-PAGE and blotted for puromycinylation, VASP as a protrusion marker, H2AX as a cell body marker, and GAPDH as loading control.

(B) Protrusions initiate but retract in translation-inhibited cells. MDA-MB231 mKate-CAAX cells were seeded on 3-μm transwells in presence or absence of cycloheximide (10 μg/ml), fixed at indicated times, and analyzed by confocal microscopy. Images show protrusions at the bottom of transwell filters. Red, cell membranes; blue, filter. Scale bar, 50 μm. See also Movie S3.

(C) Quantification of protrusions from (B) (n = 4). The significant p values are stated above the bar graph. Error bars are SD.

(D) Translation inhibition switches cell morphology from protrusive to round in 3D. MDA-MB231 cells were seeded on top of 3D collagen-I gels for 4 hr and treated with cycloheximide (10 μg/ml) for indicated times before being fixed and imaged. Scale bar, 50 μm. See also Movie S4.

(E) Quantification of protrusive versus round morphologies from (D) (n = 3). Significant p values are stated above each bar graph. Error bars are SD.

(F) Local inhibition of translation in protrusions. MDA-MB231 cells were seeded on 3-μm transwells for 2 hr. Emetine (1 μg/ml) was then added to the bottom chamber for 5 min as in Figure S2F. Transwells were then washed and treated with Puromycin (10 μg/ml) for 10 min to label nascent proteins before lysis. Equal amounts of isolated protrusion and cell body fractions were then resolved by SDS-PAGE and blotted for puromycinylation, VASP (protrusion marker), H2AX (cell body marker), and GAPDH (loading control). The emetine treatment specifically inhibits translation in protrusions.

(legend continued on next page)

protein translation. Emetine concentrations as low as 1 μg/ml, and treatment times as short as 5 min could strongly abrogate translation in MDA-MB231 cells (Figures S2D and S2E). To locally inhibit translation in protrusions, a low dose of 1 μg/ml emetine was added to the bottom of transwell filters for 5 min. In order to limit emetine diffusion upward, a positive hydrostatic pressure was generated to push liquid down from the top to the bottom of the filter (Figures S2F and S2G), allowing inhibition of translation in protrusions while leaving the cell-bodies unaffected (Figures 3F and S2H). Importantly, this local inhibition of translation also destabilized protrusions (Figures 3G and 3H; Movie S5), demonstrating that local translation is critical for the stability of protrusions.

Specific 3′UTR Motifs Are Associated with Local Translation

Despite the presence of mRNA in protrusions being a logical prerequisite for any localized translation, our results showed little correlation between mRNA and protein distributions. We hypothesized that this might be due to some protrusion-localized mRNAs remaining translationally inactive in protrusions. In support of this, mRNA and relative translation rate distributions between protrusions and the cell body negatively correlate with each other (Figure 4A). Furthermore, 2D annotation enrichment analysis revealed that most protein categories also show a negative correlation between their mRNA and translation distributions (Figure 4B), with actin cytoskeleton-associated protein categories having relatively high protrusion translation levels but low mRNA enrichments, while mitochondrial, as well as RNA-binding and ribosomal proteins have high relative protrusion mRNA levels but low relative translation in protrusions (Figure 4B; Data S2A). Collectively, these results suggest that for certain categories of mRNAs, targeting to protrusion may serve as a mechanism for translation repression, while for others, low-level mRNA presence in protrusion maybe enough to support robust local translation.

As mRNA enrichment in protrusions does not define local translation rates, we next set out to reveal the properties in mRNA sequence that may be governing whether an mRNA is locally translated or repressed in protrusions. *Cis*-regulatory elements in the 5′ and 3′ UTRs of mRNAs play a pivotal role in regulation of translation (Grillo et al., 2010). Thus, we investigated whether presence or absence of specific UTR motifs could be-associated with differences local translation rates. We focused on 58 well-known 5′ and 3′ UTR regulatory elements (Grillo et al., 2010) (Data S2B) and asked whether presence or absence of any of these elements was-associated with local translation in protrusions. We found six elements that were significantly-associated with higher local translation in protrusions (Figure 4C). The best characterized of these elements is Musashi binding element (MBE), the binding element for MSI1, which can act as both activator and inhibitor of translation depending on the context (Charlesworth et al., 2006). Interestingly, MSI1 has recently been demonstrated to bind to and regulate ARP2/3 subunits mRNAs in neuronal cells (Hadziselimovic et al., 2014), a role in agreement with its involvement in protrusions. Existence of an association between specific UTR motifs and local translation rates suggests that such motifs are likely to be locally controlling translation in protrusions.

KH, PH, and Sm Domain-Containing RBPs Modulate Protrusions

As translation is mainly governed by different RBPs and translation factors that act upon an mRNA, RBPs that are localized to protrusions are likely to be crucial for local regulation of translation. Thus, to reveal RBPs that are functionally important for protrusions, we performed an RNAi screen for protrusion-enriched RBPs. Category enrichment analysis revealed three families of RBPs that were significantly enriched in protrusions (Data S1B). These were Sm, KH, and RNase PH domain-containing proteins (Figures 5A–5C). As enrichment of multiple structurally related proteins can be indicative of a conserved function, we focused on the members of these categories, depleting each protein by RNAi and assessing the ability of depleted cells to form stable protrusions through transwell filters. Out of a total of 38 RBPs screened, knockdown of 17 significantly impacted on protrusions (Figure 5D). Interestingly, while the majority of knockdowns inhibited protrusions, some enhanced them (Figure 5D), suggesting that different protrusion localized RBPs function in opposite manners to fine-tune protrusion dynamics.

To further validate the role of these RBPs in mesenchymal-like migration, we assessed the invasion of MDA-MB231 cells through a 3D collagen-I matrix, where they preferentially migrate as mesenchymal-like cells, following siRNA depletion. Strikingly, knockdown of 16 out of the 17 RBP hits significantly impaired the invasive potential of MDA-MB231 cells (Figure 5D), suggesting that most of these RBPs are likely to play a role in regulation of mesenchymal-like cell migration in 3D. Interestingly, RBP knockdown of both negative as well as positive regulators of protrusions had a negative impact on the invasive potential of the cells (Figure 5D), suggesting that a precise fine tuning of protrusion formation is crucial for optimal migration in 3D.

Several of the identified RBPs such as the fragile X mental retardation protein-1 (FMR1) and its two homologs (FXR1 and FXR2), zipcode-binding proteins (IGF2BP2 and IGF2BP3), heterogeneous nuclear ribonucleoprotein K (HNRPK), and small nuclear ribonucleoprotein core subunits (SNRPD1, SNRPD3, SNRPF, SNRPG), have been reported to regulate mRNA localization or local translation (Boudoukha et al., 2010; Comery et al., 1997; Gu et al., 2012; Liu et al., 2008; Nielsen et al., 2001; Schaeffer et al., 2012; Taniuchi et al., 2014; Vasudevan and Steitz, 2007; Zalfa et al., 2006; Zhang et al., 1995). Others such as vigilin (VGL), partner of NOB1 (PNO1), and ribosomal protein subunit-3 (RPS3), either associate with, or are part of the translation machinery itself (Kim et al., 2010; Kruse et al., 2003; Vanrobays et al., 2004). However, a number of the

(G) Inhibition of translation in protrusions destabilizes protrusions. MDA-MB231 mKate-CAAX cells were seeded on 3-μm transwells for 2 hr before being treated with emetine (1 μg/ml) or vehicle as in (F). The cells were then either fixed immediately (0 min), or left for 1 hr (60 min) before being fixed and analyzed by confocal microscopy. The images show protrusions at the bottom of the filter. Red, cell membranes; blue, filter. Scale bar, 50 μm. See also Movie S5.
(H) Quantification of protrusions from (G) (n = 10). The significant p values are stated above the bar graph. Error bars are SD.
See also Figure S2.

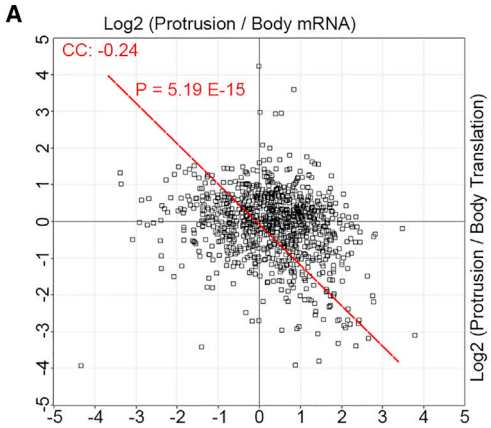

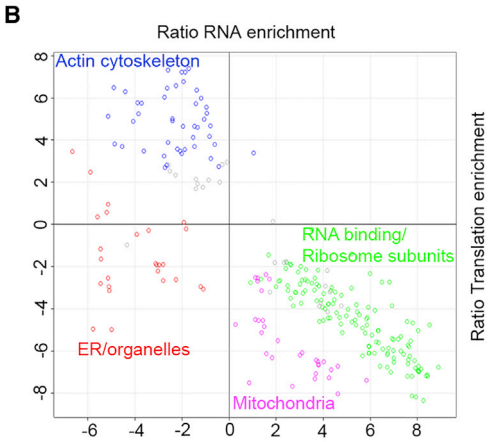

C

UTR	Element name	size	Benj. Hoch. FDR	Median
3'	ADH_DRE	13	0.0380786	0.646664
3'	SECIS1	6	0.0444617	0.514125
3'	BRD-BOX	60	0.106622	0.337944
3'	SXL_BS	110	0.0205958	0.193567
3'	K-BOX	109	0.106389	0.166405
3'	MBE	338	0.00119489	0.121955

Figure 4. mRNA Enrichment Does Not Determine Local Translation Rates in Protrusions

(A) mRNA distributions between protrusions and the cell body negatively correlate with translation rate distributions. Averaged Log2 of protrusion/cell body mRNA FPKM ratios from two replicate experiments were plotted against averaged Log2 of protrusion/cell body pSILAC translation ratios. CC, Pearson's correlation coefficient. P value of the correlation is displayed on the graph.

(B) Most categories of proteins show a negative correlation between their mRNA localization and local translation. The 2D-annotation enrichment analysis data from Data S2A was plotted with each data point representing a protein category. Most actin cytoskeleton-related categories (blue) show high relative local translation rates but their mRNA is not highly enriched in protrusions while mitochondrial (purple) and RNA-binding/ribosomal (green) protein categories show high relative mRNA enrichment but low local translation rates in protrusions. mRNAs for ER and other organelle categories (red) are enriched and translated more in the cell body.

(C) Specific 3′ UTR elements are associated with higher local translation rates in protrusions. Data of averaged Log2 of protrusion/cell body pSILAC translation ratios were annotated for known UTR elements from UTRdb (Grillo et al., 2010) (see also Data S2B), and subjected to 1D annotation enrichment analysis. Six UTR elements were significantly enriched in locally translated mRNAs as listed. Size, the number of mRNAs annotated with each element in the dataset; Benj. Hoch. FDR, Benjamini Hochberg false detection rate for enrichments; median, median of the averaged Log2(protrusion/cell body) pSILAC translation ratios for each UTR category.

identified proteins were not previously implicated in regulation of local translation, including three subunits of the exosome core complex (EXOSC7, EXOSC8, and EXOSC9), an RNA degrading complex involved in maturation, quality control, and turnover of many types of cellular RNA (Lykke-Andersen et al., 2009) (Figure 5D), suggesting that they are likely to be novel regulators of local translation in protrusions.

The Exosome Complex Is a Regulator of Cell Protrusions, Morphology, and Migration

To further expand on our results, we validated the role of the exosome core in protrusions, as a potential regulator of local translation and protrusion formation. The exosome core consists of nine subunits that assemble into a two-layered barrel-like structure, with the upper layer forming a cap of three subunits that sit on a ring of six RNase PH domain-containing subunits (Liu et al., 2006). In mammalian cells, the exosome core is catalytically inactive but peripherally associates with a set of catalytically active 3′-5′ exoribonuclease subunits that mediate RNA processing/degradation events (Lykke-Andersen et al., 2009). Although only six subunits of the exosome core were initially included in our screen, we found all of the nine exosome core subunits to be present and more abundant in protrusions than the cell body, with eight out of nine showing at least 2-fold enrichment (Figure 6A). Surprisingly, RRP6 and DIS3, the two catalytic subunits of the exosome that were expressed in our cells, were significantly depleted in protrusions (Figure 6A), suggesting that the activity of the exosome core in protrusions might be independent of the catalytic subunits.

First, we confirmed the enrichment of exosome core in protrusions of MDA-MB231 cells by western blotting. In agreement with the proteomics data, western blot analysis of protrusion and cell body fractions with antibodies against exosome core confirmed a high level of enrichment in protrusions, while blotting for the catalytic subunits showed a strong enrichment in the cell body (Figure 6B). Specificity of the antibodies was validated by RNAi (Figure S3A). Accordingly, immunofluorescence analysis showed a fraction of exosome core that was localized to the leading edge, while the two catalytic subunits of the exosome were enriched in the nucleus (Figure 6C). Next, using RNAi, we depleted each exosome core subunit and assessed the ability of depleted cells to form protrusions through 3-μm transwell filters. Efficient depletion of different exosome core subunits was evaluated by qPCR (Figure S3B), and mass spectrometry (Figure S3C). No apoptosis or change in cell proliferation could be detected upon depletion of exosome core subunits over 72 hr (Figures S3D and S3E), suggesting that transient depletion of the exosome core does not impact cell viability. In these settings, knockdown of seven out of nine exosome core subunits significantly inhibited protrusions (Figures 6D and 6E). Depletion of exosome core subunits also inhibited protrusions in HT-1080 fibrosarcoma cells (Figures S3F and S3G), without impacting cell viability (data not shown), suggesting that the role of the exosome in protrusions is not cell type-specific. Importantly,

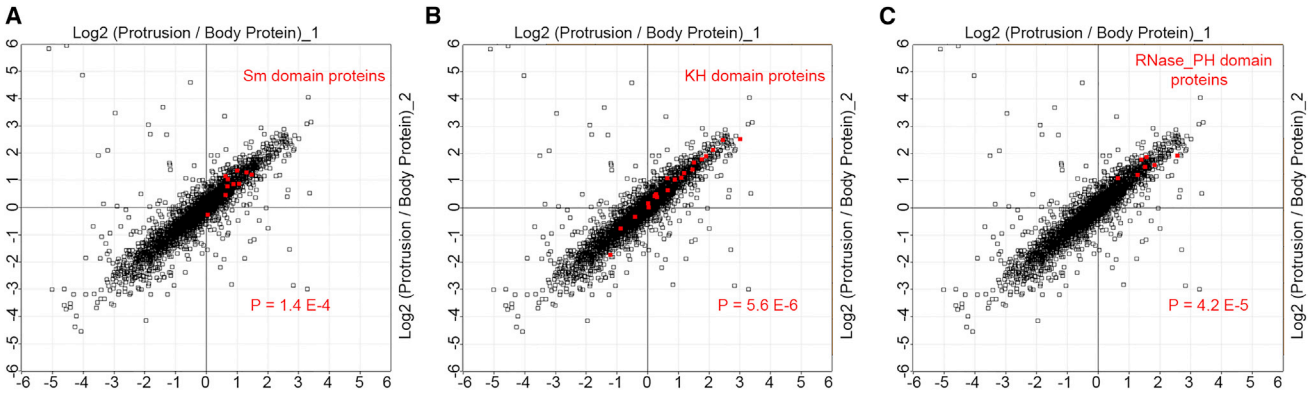

D

Protein name	Domain	Effect on protrusions	p-value	Effect on 3D invasion	p-value
EXOSC7	RNase_PH	inhibition	3.5 E-03	inhibition	4.1E-06
EXOSC8	RNase_PH	inhibition	3.5 E-04	inhibition	1.6E-04
EXOSC9	RNase_PH	inhibition	4.8 E-03	inhibition	4.0E-05
FMR1	KH	inhibition	1.3 E-03	inhibition	8.0E-03
FXR1	KH	inhibition	1.3 E-03	inhibition	2.4E-02
FXR2	KH	inhibition	4.1 E-05	inhibition	4.5E-04
VGL	KH	enhancement	1.6 E-04	inhibition	4.1E-03
HNRPK	KH	inhibition	2.9 E-03	inhibition	3.1E-06
IGF2BP2	KH	enhancement	2.4 E-06	inhibition	3.0E-02
IGF2BP3	KH	enhancement	5.2 E-03	inhibition	1.5E-07
PCBP1	KH	inhibition	7.2 E-03	inhibition	3.8E-02
PNO1	KH	inhibition	1.5 E-05	inhibition	1.8E-02
RPS3	KH	inhibition	3.7 E-06	no effect	0.72
SNRPD1	Sm	inhibition	3.1 E-04	inhibition	3.1E-02
SNRPD3	Sm	inhibition	3.4 E-03	inhibition	3.4E-09
SNRPF	Sm	inhibition	8.0 E-03	inhibition	4.0E-02
SNRPG	Sm	inhibition	7.7 E-05	inhibition	1.8E-06

Figure 5. Specific Categories of RBPs Are Enriched in and Functionally Important for Protrusions

(A) Sm domain-containing RBPs are significantly enriched in protrusions. Log2 of SILAC-quantified protein ratios were plotted against each other with all Sm domain proteins marked in red. P value for the annotation enrichment is displayed on the graph.

(B) KH domain-containing RBPs are significantly enriched in protrusions. Log2 of SILAC-quantified protein ratios were plotted against each other with all KH domain proteins marked in red. P value for the annotation enrichment is displayed on the graph.

(C) RNase PH domain-containing RBPs are significantly enriched in protrusions. Log2 of SILAC-quantified protein ratios were plotted against each other with all RNase PH domain proteins marked in red. P value for the annotation enrichment is displayed on the graph.

(D) List of all significant hits from RNAi screening of protrusion-enriched RBPs in MDA-MB231 mKate-CAAX cells, their depletion effect on protrusions (inhibition or enhancement), as well as their depletion effect on 3D invasion into collagen-I. First p value column is for the t test significance of the change in protrusions. Second p value column is for the t test significance of the change in 3D invasion index.

analysis of protrusion dynamics by time-lapse microscopy revealed that similar to inhibition of local translation, exosome core depletion did not affect protrusion initiation, but resulted in destabilization of already initiated protrusions (Movie S6). Exosome depletion also destabilized protrusions in 3D collagen-I matrix, resulting in conversion of the cells from a polarized mesenchymal-like morphology to round (Figures 6F and 6G; Movie S7). As expected, the invasion of MDA-MB231 cells through 3D collagen-I matrix was also significantly impaired upon depletion of several exosome core subunits (Figures 6H and 6I). Together, these results reveal that the exosome core subunits, but not the catalytic subunits, are enriched in protrusions and are necessary for protrusion stabilization, mesenchymal-like morphology, and migration in 3D.

DISCUSSION

By comparing the differences between protrusions and the cell body in distribution of proteins, mRNAs, and their relative translation rates, we show that localized translation contributes significantly toward protein localization to protrusions (Figures 2G and 2I). In fact, for the majority of actin-related protein categories enriched in protrusions, such as drivers of actin polymerization, adhesion regulators, and most actin-binding proteins, localized translation seems to be a crucial determinant of protein localization to protrusions (Figure 2H; Data S1E). However, unlike actin-related proteins, RBPs and ribosomal proteins exhibit much higher relative protein levels in protrusions compared to their relative local translation rates (Figure 2H; Data S1E), suggesting that their localization to protrusions must be independent of local synthesis and thus defined by transport. In case of the majority of ribosomal proteins, this is not surprising as regardless of where they may be synthesized in the cytoplasm, they would have to be first transported to the nucleus where they associate with rRNAs in order to form the ribosome subunits (Kressler et al., 2010). Mature ribosome subunits then need to be transported to other cellular destinations to carry out translation. By analogy, the fact that RBPs are not locally translated either suggests that they may

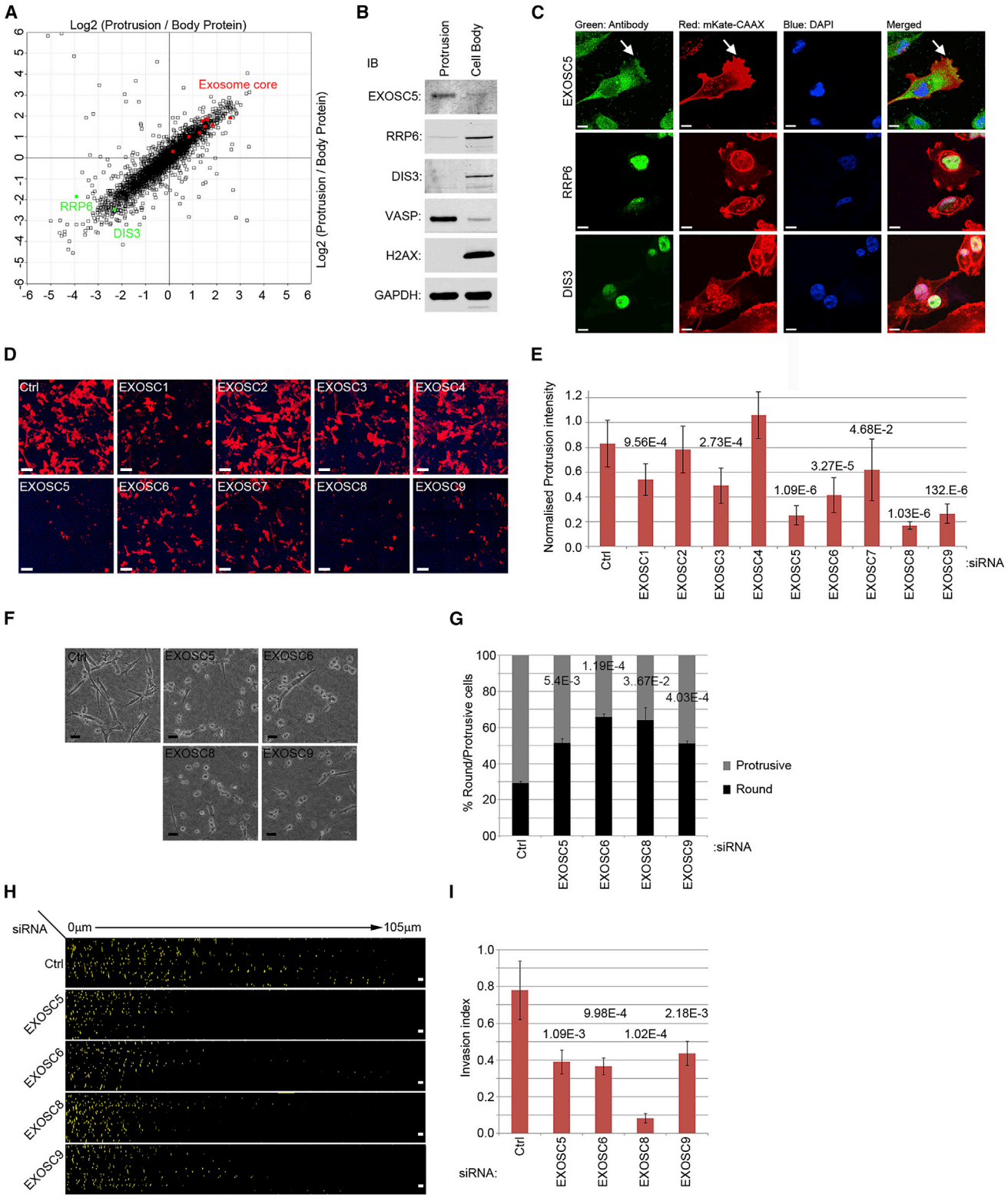

Figure 6. Exosome Core Is Enriched in Protrusions and Is Required for Protrusion Stability, Mesenchymal-like Morphology, and 3D Migration

(A) Exosome core subunits, but not catalytic subunits, are enriched in protrusions. Log2 of SILAC-quantified protein ratios were plotted against each other with exosome core subunits marked in red and catalytic subunits in green. All nine exosome core subunits were present more in protrusions than the cell body with eight showing at least 2-fold enrichment, while both expressed catalytic subunits show a strong enrichment in the cell body.

(legend continued on next page)

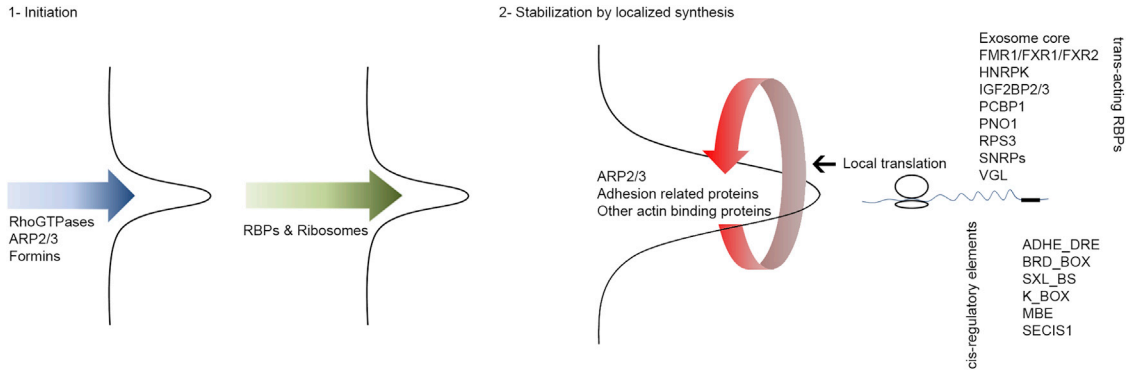

Figure 7. Two-Step Model for Regulation of Protrusion Formation by Local Translation

Protrusions are initiated by the action of actin regulators such as Rho-GTPases, which promote actin polymerization via ARP2/3 complex and formins. Once initiated, ribosomes and RBPs in complex with their target mRNAs are transported to protrusions where they mediate local synthesis of more actin-associated proteins, resulting in protrusion stabilization and growth. Local translation rates in protrusions are defined, not by mRNA enrichment alone, but via specific mRNA *cis*-regulatory UTR elements and *trans*-acting RBPs enriched in protrusions.

be pre-associated with their target mRNAs before transport to protrusions. Considering this, and as we show that the role of localized translation is to stabilize already initiated protrusions (Figures 3B–3H; Movies S3, S4, and S5), we propose a two-step model for protrusion formation in which ribosomes and specific RBPs in complex with their associated mRNAs are transported to sites of protrusions following protrusion initiation, where their localized activity increases translation of actin cytoskeletal proteins, resulting in further growth and stabilization of already initiated protrusions (Figure 7).

Importantly, we show that mRNA distributions do not correlate with protein distributions between protrusions and the cell body (Figure 2D). In fact, several categories of locally translated proteins in protrusions do not seem to exhibit any mRNA enrichment (Figure 4B). Conversely, several categories of protrusion-enriched mRNAs have low relative translation rates in protrusions, suggestive of their local repression (Figure 4B). These include mitochondrial as well as RNA-binding and ribosomal protein categories, which show a strong enrichment of their mRNAs in protrusions, but these localized mRNAs seem to be translationally repressed (Figure 4B). Regulated translational repression of localized mRNAs has been shown before (Buxbaum et al., 2014; Hüttelmaier et al., 2005). For instance, zipcode binding protein IGF2BP1, which is crucial for targeting β-actin mRNA, also represses translation, but this translational repression can be relieved with the right signal, which in case of IGF2BP1 is phosphorylation at the leading edge by the tyrosine kinase SRC (Hüttelmaier et al., 2005). A similar model may apply to the categories of locally repressed mRNAs defined in this study, which would mean that their local translation could be switched on, following yet unidentified cellular signals. Alternatively, for certain categories of mRNAs, localization to protrusion could be functioning as a means of global translation suppression by keeping them away from their correct site of translational activity in the cell body.

Nevertheless, the lack of a positive correlation between mRNA localization and local translation (Figures 4A and 4B) suggests that the level of mRNA accumulation may not be a good predictor for local translation. A few copies of certain localized mRNAs may be able to support robust levels of local translation, while high levels of localization for other mRNAs may not lead to significant local translation. Although it is possible that our findings may mostly apply to immortalized, transformed, or malignant cells such as the one that was used here, these findings still have important ramifications for RNA localization studies as they highlight that mRNA

(B) Western blot analysis of exosome core and catalytic subunits enrichments in protrusion and cell body fractions of MDA-MB231 cells. Equal amounts of isolated protrusion and cell body fractions were resolved by SDS-PAGE and blotted for EXOSC5, RRP6, DIS3, as well as VASP (protrusion marker), H2AX (cell body marker) and GAPDH (loading control). While EXOSC5 shows a strong enrichment in protrusion fraction, RRP6 and DIS3 show enrichment in the cell body.
(C) Immunofluorescence analysis of exosome core and catalytic subunits localizations. MDA-MB231 mKate-CAAX cells seeded on top of collagen-I coated coverslips were fixed and stained with indicated antibodies. A fraction of EXOSC5 localizes to the leading edge of the cells, while RRP6 and DIS3 are mostly nuclear.
(D) RNAi-mediated depletion of exosome core subunits inhibits protrusions. MDA-MB231 mKate CAAX cells were transfected with indicated siRNAs. After 72 hr, the cells were seeded on top of transwell filters for 4 hr before being fixed and analyzed by confocal microscopy. Images show protrusions at the bottom of the filter. Red, cell membranes; blue, filter. Scale bar, 50 μm. See also Movie S6.
(E) Quantification of protrusions from (D) (n = 10). Significant p values are stated above each bar graph. Error bars are SD.
(F) Exosome core depletion switches MDA-MB231 cell morphology from protrusive to round. MDA-MB231 cells were transfected with indicated siRNAs before being seeded on top of a thick 3D collagen-I matrix 72 hr post-transfection. Cells were imaged 24 hr after seeding. Scale bar, 50 μm. See also Movie S7.
(G) Quantification of the percentage of protrusive versus round cells from F (n = 3). Significant p values are stated above each bar graph. Error bars are SD.
(H) Inhibition of 3D invasion by knockdown of four different exosome core subunits. MDA-MB231 cells were transfected with indicated siRNAs. After 72 hr, the cells were allowed to invade through a collagen matrix. Cells were labeled 24 hr prior to invasion analysis by CellTracker-CMRA (orange). Z stack images were taken at 5-μm intervals and put together serially from 0 μm to 105 μm. Scale bar, 200 μm.
(I) Quantification of 3D invasion analysis from (H) (n = 6). Significant p values are stated above each bar graph. Error bars are SD. See also Figure S3.

localization alone may not be an indicator for local protein expression by default.

As mRNA translation is chiefly regulated by *cis*-regulatory elements within 5′ and 3′ UTRs of mRNAs, we investigated the association of different known UTR elements with regulation of local translation in protrusions. Our study reveals that presence of specific 3′ UTR elements is associated with higher local translation rates in protrusions (Figure 4C). The exact functions of these regulatory motifs in control of local translation in protrusions remain to be determined. It also remains to be determined if there are yet unknown UTR elements associated with local translation in protrusions, in addition to the known UTR elements investigated here.

To reveal functionally important RBP regulators of localized translation in protrusion, we performed an RNAi screen, depleting members of RBP categories significantly enriched in protrusions and assessing whether their depletion modulated protrusions. Out of 38 RBPs screened, we identified 17 belonging to different categories that significantly regulated protrusions. Sixteen out of 17 also significantly affected migration in 3D collagen-I matrix (Figure 5D). Many of these RBPs have been reported to regulate RNA localization or local translation. However, a number of proteins we identified, including exosome core subunits, have not been implicated in regulation of RNA targeting or local translation. Previously, the exosome core was shown to be present in both the nucleus and cytosol of eukaryotic cells (Lykke-Andersen et al., 2009), although tagging approaches in *Drosophila* had also suggested presence of certain exosome subunits in the periphery of the cells (Graham et al., 2006). Our data reveal that, at least in a mesenchymal-like highly invasive cancer cell-line, the exosome core, but not its catalytic subunits, is enriched in protrusions (Figures 6A–6C) and acts to stabilize protrusions and promote 3D invasion (Figures 6D–6I; Movies S6 and S7). As cell migration and invasion are believed to be intimately linked with metastasis, the exosome-mediated regulation of mesenchymal-like cell migration described here may impact cancer metastasis. In support of this view, we found that, in human breast cancers, increased expression of the exosome core subunits correlates with bad prognosis. This was the case with every exosome core subunit for which expression data were available (Curtis et al., 2012) (Figures S3H–S3L). This result implicates the exosome core in cancer progression and raises the possibility that regulation of cell migration via the exosome could be resulting in a more aggressive, metastatic phenotype.

It is now evident that many types of non-coding RNAs such as microRNAs, long non-coding RNAs, and anti-sense RNAs play a significant role in post-transcriptional regulation of mRNA expression. It is therefore likely that in addition to RNA-binding proteins, non-coding RNAs may also be involved in regulation of local translation in protrusions. In fact, two of the known *cis*-regulatory elements (K-BOX, BRD-BOX) identified here as associated with higher protrusion translation rates, are not known to bind to any RBPs but instead seem to associate with microRNAs (Lai et al., 2005). As our RNA-seq analysis was limited to mRNAs, it remains to be determined whether certain non-coding RNAs also show enrichment in protrusions, and more importantly, whether they play a functional role in regulating protrusions.

EXPERIMENTAL PROCEDURES

Transwell Protrusion, 3D Collagen Invasion, and 3D Collagen Morphology Assays

3D collagen invasion assay and 3D collagen morphology assays were done as described before (Sanz-Moreno et al., 2008) with modifications (see also Supplemental Experimental Procedures). Transwell protrusion formation assays were performed on 3-μm pore transwell filters (6.5 mm insert size, 24-well format), coated with 5 μg/ml collagen. A total of 100,000 cells were seeded in 100 μl serum-free DMEM on top of the filter and 600 μl of DMEM with 10% serum was placed in the bottom chamber. Cells were imaged live, or fixed with 4% formaldehyde at indicated time points before imaging. Multiple tile scans, from at least three independent experiments, each composed of 3 × 3 contiguous fields of view, were taken at two z planes (top and bottom of the filter). For quantification of protrusions, fluorescence intensity at the bottom and top of the filter was then measured by ImageJ and bottom to top ratio was calculated.

Translation Inhibition and Puromycinylation

For puromycinylation of nascent proteins, cells were treated with 10 μg/ml puromycin for 10 min prior to lysis. For cycloheximide treatments, 10 μg/ml cycloheximide was added to the cells for indicated times. For emetine treatments, indicated dose of emetine was added to the cells for indicated times, followed by a single wash in 10% FBS containing DMEM. For specific inhibition of translation in protrusions, cells were seeded on transwells and allowed to form protrusions for 2 hr. The transwells were transferred to a reservoir dish with 1 μg/ml emetine (or vehicle for control treatment) in 10% FBS containing DMEM. The level of liquid in the reservoir was always significantly lower than on top of the filter, creating a positive hydrostatic pressure that limited emetine diffusion upward. After 5 min, the filters were taken out, washed by dipping the filter in 10% FBS containing DMEM, and transferred back to the original well for downstream analysis.

Protrusion Purification

Purification of cell protrusions was performed using 3-μm pore polycarbonate transwell filters (75 mm membrane inserts). Filters were coated with 5 μg/ml collagen before being seeded with 10 million cells in serum-free DMEM on top, with DMEM containing 10% serum added to the bottom. For western blot analysis, a single transwell was used per condition. For proteomics analysis, four transwells were used per condition. After allowing the cells to form protrusions for 2 hr, transwells were washed in PBS, fixed with −20°C methanol for 20 min, washed again with PBS, and the protrusions from the bottom of the filter were shaved off using a glass coverslip, with the coverslip being dipped in 2% SDS sample buffer. The cell body fraction was then prepared by direct addition of sample buffer to the top of the filter. A similar procedure was used for RNA purification from protrusions, but from one transwell per condition, no methanol fixing, and lysing in RLT buffer from QIAGEN's RNeasy Mini Kit. RNA was purified according to the manufacturer's instructions, followed by spectrophotometric measurement of the quality and concentrations.

Proteomics/Transcriptomics Analysis

For SILAC labeling, cells were grown for seven doublings in heavy or light SILAC DMEM supplemented with 10% dialyzed FBS and 600 mg/l L-Pro. For pSILAC, light-labeled cells were transiently switched to medium or heavy SILAC DMEM during a 2-hr transwell protrusion formation assay. Reciprocally mixed SILAC or pSILAC samples were resolved by SDS-PAGE, stained with Gel-code blue Coomassie dye (Pierce), and cut into 23 sections before Trypsin digestion and peptide extraction. Liquid chromatography-tandem mass spectrometry (LC-MS/MS) analysis was performed by the Institute of Cancer Research (ICR) proteomics core facility. Mass spectrometry search and quantifications were done by Maxquant software (Cox and Mann, 2008; Cox et al., 2011). For pSILAC quantifications, the L label was ignored and H/M ratios, which measure relative nascent protein levels, were used. For RNA-seq, protrusions and the cell body total RNA preps were generated in duplicates from two biological filter-fractionated replicate experiments. Sample preparations and Illumina sequencings were performed by ICR's tumor profiling unit. All proteomics/transcriptomics data analyses were performed by Perseus software (Cox and Mann, 2012) (see also Supplemental Experimental Procedures).

Mass spectrometry proteomics raw data and search results were deposited to the ProteomeXchange Consortium (Vizcaíno et al., 2014), via the PRIDE partner repository, with the dataset identifiers PRIDE: PXD000914 and PRIDE: PXD002649. RNA-seq data were deposited to the ArrayExpress database (http://www.ebi.ac.uk/arrayexpress) under the accession number ArrayExpress: E-MTAB-2546.

ACCESSION NUMBERS

The accession numbers for the mass spectrometry proteomics raw data and search results reported in this paper are PRIDE: PXD000914 and PXD002649. The accession number for the RNA-seq data reported in this paper is ArrayExpress: E-MTAB-2546.

SUPPLEMENTAL INFORMATION

Supplemental Information includes Supplemental Experimental Procedures, three figures, seven movies, and two Supplemental Data files and can be found with this article online at http://dx.doi.org/10.1016/j.devcel.2015.10.005.

AUTHOR CONTRIBUTIONS

F.K.M. and C.J.M. designed all experiments and wrote the manuscript. A.P. assisted with mass spectrometry sample preps and LC-MS/MS runs. H.P. generated the MDA-MB231 mKate CAAX cell line and assisted with confocal microscopy. A.S. assisted with immunofluorescence. S.K. assisted with 3D live-cell imaging. A.M. assisted with exosome validation experiments. Y.Y. performed the gene expression-based stratification of the breast cancer patient survival data. All other experiments and data analyses were performed by F.K.M.

ACKNOWLEDGMENTS

We would like to thank Annette Self for help with experiments, reagents, and protocols, Andreas Hadjiprocopis and James Campbell for help with bioinformatics analysis, Hani Goodarzi for advice on UTR analysis, Graziano Pesole for assistance with UTRdb, ICR's proteomics core facility for mass spectrometry runs, and ICR's tumor profiling unit for RNA-seq sample preparations and sequencings. Ger Pruijn generously provided for EXOSC5 antibody. Finally, we would like to thank C.J.M. lab members for their comments and discussions. This work was funded by Cancer Research UK (C107/A12057, C107/A10433, C107/A16512).

Received: April 24, 2015
Revised: August 23, 2015
Accepted: October 8, 2015
Published: November 9, 2015

REFERENCES

Boudoukha, S., Cuvellier, S., and Polesskaya, A. (2010). Role of the RNA-binding protein IMP-2 in muscle cell motility. Mol. Cell. Biol. *30*, 5710–5725.

Buxbaum, A.R., Wu, B., and Singer, R.H. (2014). Single β-actin mRNA detection in neurons reveals a mechanism for regulating its translatability. Science *343*, 419–422.

Cain, R.J., and Ridley, A.J. (2009). Phosphoinositide 3-kinases in cell migration. Biol. Cell *101*, 13–29.

Charlesworth, A., Wilczynska, A., Thampi, P., Cox, L.L., and MacNicol, A.M. (2006). Musashi regulates the temporal order of mRNA translation during Xenopus oocyte maturation. EMBO J. *25*, 2792–2801.

Comery, T.A., Harris, J.B., Willems, P.J., Oostra, B.A., Irwin, S.A., Weiler, I.J., and Greenough, W.T. (1997). Abnormal dendritic spines in fragile X knockout mice: maturation and pruning deficits. Proc. Natl. Acad. Sci. USA *94*, 5401–5404.

Condeelis, J., and Singer, R.H. (2005). How and why does beta-actin mRNA target? Biol. Cell *97*, 97–110.

Cox, J., and Mann, M. (2008). MaxQuant enables high peptide identification rates, individualized p.p.b.-range mass accuracies and proteome-wide protein quantification. Nat. Biotechnol. *26*, 1367–1372.

Cox, J., and Mann, M. (2012). 1D and 2D annotation enrichment: a statistical method integrating quantitative proteomics with complementary high-throughput data. BMC Bioinformatics *13* (*Suppl 16*), S12.

Cox, J., Neuhauser, N., Michalski, A., Scheltema, R.A., Olsen, J.V., and Mann, M. (2011). Andromeda: a peptide search engine integrated into the MaxQuant environment. J. Proteome Res. *10*, 1794–1805.

Crawford, A.W., Michelsen, J.W., and Beckerle, M.C. (1992). An interaction between zyxin and alpha-actinin. J. Cell Biol. *116*, 1381–1393.

Curtis, C., Shah, S.P., Chin, S.F., Turashvili, G., Rueda, O.M., Dunning, M.J., Speed, D., Lynch, A.G., Samarajiwa, S., Yuan, Y., et al.; METABRIC Group (2012). The genomic and transcriptomic architecture of 2,000 breast tumours reveals novel subgroups. Nature *486*, 346–352.

Etienne-Manneville, S. (2008). Polarity proteins in migration and invasion. Oncogene *27*, 6970–6980.

Graham, A.C., Kiss, D.L., and Andrulis, E.D. (2006). Differential distribution of exosome subunits at the nuclear lamina and in cytoplasmic foci. Mol. Biol. Cell *17*, 1399–1409.

Grillo, G., Turi, A., Licciulli, F., Mignone, F., Liuni, S., Banfi, S., Gennarino, V.A., Horner, D.S., Pavesi, G., Picardi, E., and Pesole, G. (2010). UTRdb and UTRsite (RELEASE 2010): a collection of sequences and regulatory motifs of the untranslated regions of eukaryotic mRNAs. Nucleic Acids Res. *38*, D75–D80.

Gu, W., Katz, Z., Wu, B., Park, H.Y., Li, D., Lin, S., Wells, A.L., and Singer, R.H. (2012). Regulation of local expression of cell adhesion and motility-related mRNAs in breast cancer cells by IMP1/ZBP1. J. Cell Sci. *125*, 81–91.

Hadziselimovic, N., Vukojevic, V., Peter, F., Milnik, A., Fastenrath, M., Fenyves, B.G., Hieber, P., Demougin, P., Vogler, C., de Quervain, D.J., et al. (2014). Forgetting is regulated via Musashi-mediated translational control of the Arp2/3 complex. Cell *156*, 1153–1166.

Halstead, J.M., Lionnet, T., Wilbertz, J.H., Wippich, F., Ephrussi, A., Singer, R.H., and Chao, J.A. (2015). An RNA biosensor for imaging the first round of translation from single cells to living animals. Science *347*, 1367–1671.

Hüttelmaier, S., Zenklusen, D., Lederer, M., Dictenberg, J., Lorenz, M., Meng, X., Bassell, G.J., Condeelis, J., and Singer, R.H. (2005). Spatial regulation of beta-actin translation by Src-dependent phosphorylation of ZBP1. Nature *438*, 512–515.

Kim, H.D., Kim, T.S., Joo, Y.J., Shin, H.S., Kim, S.H., Jang, C.Y., Lee, C.E., and Kim, J. (2010). RpS3 translation is repressed by interaction with its own mRNA. J. Cell. Biochem. *110*, 294–303.

Kressler, D., Hurt, E., and Bassler, J. (2010). Driving ribosome assembly. Biochim. Biophys. Acta *1803*, 673–683.

Kruse, C., Willkomm, D., Gebken, J., Schuh, A., Stossberg, H., Vollbrandt, T., and Müller, P.K. (2003). The multi-KH protein vigilin associates with free and membrane-bound ribosomes. Cell. Mol. Life Sci. *60*, 2219–2227.

Lai, E.C., Tam, B., and Rubin, G.M. (2005). Pervasive regulation of Drosophila Notch target genes by GY-box-, Brd-box-, and K-box-class microRNAs. Genes Dev. *19*, 1067–1080.

Liu, Q., Greimann, J.C., and Lima, C.D. (2006). Reconstitution, activities, and structure of the eukaryotic RNA exosome. Cell *127*, 1223–1237.

Liu, Y., Gervasi, C., and Szaro, B.G. (2008). A crucial role for hnRNP K in axon development in Xenopus laevis. Development *135*, 3125–3135.

Lykke-Andersen, S., Brodersen, D.E., and Jensen, T.H. (2009). Origins and activities of the eukaryotic exosome. J. Cell Sci. *122*, 1487–1494.

Mili, S., Moissoglu, K., and Macara, I.G. (2008). Genome-wide screen reveals APC-associated RNAs enriched in cell protrusions. Nature *453*, 115–119.

Mingle, L.A., Okuhama, N.N., Shi, J., Singer, R.H., Condeelis, J., and Liu, G. (2005). Localization of all seven messenger RNAs for the actin-polymerization

nucleator Arp2/3 complex in the protrusions of fibroblasts. J. Cell Sci. *118*, 2425–2433.

Nielsen, F.C., Nielsen, J., and Christiansen, J. (2001). A family of IGF-II mRNA binding proteins (IMP) involved in RNA trafficking. Scand. J. Clin. Lab. Invest. Suppl. *234*, 93–99.

Nobes, C.D., and Hall, A. (1995). Rho, rac, and cdc42 GTPases regulate the assembly of multimolecular focal complexes associated with actin stress fibers, lamellipodia, and filopodia. Cell *81*, 53–62.

Ong, S.E., Blagoev, B., Kratchmarova, I., Kristensen, D.B., Steen, H., Pandey, A., and Mann, M. (2002). Stable isotope labeling by amino acids in cell culture, SILAC, as a simple and accurate approach to expression proteomics. Mol. Cell. Proteomics *1*, 376–386.

Ridley, A.J. (2011). Life at the leading edge. Cell *145*, 1012–1022.

Rottner, K., Behrendt, B., Small, J.V., and Wehland, J. (1999). VASP dynamics during lamellipodia protrusion. Nat. Cell Biol. *1*, 321–322.

Sahai, E., and Marshall, C.J. (2003). Differing modes of tumour cell invasion have distinct requirements for Rho/ROCK signalling and extracellular proteolysis. Nat. Cell Biol. *5*, 711–719.

Sanz-Moreno, V., Gadea, G., Ahn, J., Paterson, H., Marra, P., Pinner, S., Sahai, E., and Marshall, C.J. (2008). Rac activation and inactivation control plasticity of tumor cell movement. Cell *135*, 510–523.

Schaeffer, V., Hansen, K.M., Morris, D.R., LeBoeuf, R.C., and Abrass, C.K. (2012). RNA-binding protein IGF2BP2/IMP2 is required for laminin-β2 mRNA translation and is modulated by glucose concentration. Am. J. Physiol. Renal Physiol. *303*, F75–F82.

Schmidt, E.K., Clavarino, G., Ceppi, M., and Pierre, P. (2009). SUnSET, a nonradioactive method to monitor protein synthesis. Nat. Methods *6*, 275–277.

Selbach, M., Schwanhäusser, B., Thierfelder, N., Fang, Z., Khanin, R., and Rajewsky, N. (2008). Widespread changes in protein synthesis induced by microRNAs. Nature *455*, 58–63.

Shankar, J., Messenberg, A., Chan, J., Underhill, T.M., Foster, L.J., and Nabi, I.R. (2010). Pseudopodial actin dynamics control epithelial-mesenchymal transition in metastatic cancer cells. Cancer Res. *70*, 3780–3790.

Small, J.V., and Resch, G.P. (2005). The comings and goings of actin: coupling protrusion and retraction in cell motility. Curr. Opin. Cell Biol. *17*, 517–523.

St Johnston, D. (2005). Moving messages: the intracellular localization of mRNAs. Nat. Rev. Mol. Cell Biol. *6*, 363–375.

Taniuchi, K., Furihata, M., Hanazaki, K., Saito, M., and Saibara, T. (2014). IGF2BP3-mediated translation in cell protrusions promotes cell invasiveness and metastasis of pancreatic cancer. Oncotarget *5*, 6832–6845.

Vanrobays, E., Gélugne, J.P., Caizergues-Ferrer, M., and Lafontaine, D.L. (2004). Dim2p, a KH-domain protein required for small ribosomal subunit synthesis. RNA *10*, 645–656.

Vasudevan, S., and Steitz, J.A. (2007). AU-rich-element-mediated upregulation of translation by FXR1 and Argonaute 2. Cell *128*, 1105–1118.

Vizcaíno, J.A., Deutsch, E.W., Wang, R., Csordas, A., Reisinger, F., Ríos, D., Dianes, J.A., Sun, Z., Farrah, T., Bandeira, N., et al. (2014). ProteomeXchange provides globally coordinated proteomics data submission and dissemination. Nat. Biotechnol. *32*, 223–226.

Wang, Y., Ding, S.J., Wang, W., Yang, F., Jacobs, J.M., Camp, D., 2nd, Smith, R.D., and Klemke, R.L. (2007). Methods for pseudopodia purification and proteomic analysis. Sci. STKE *2007*, pl4.

Wolf, K., Alexander, S., Schacht, V., Coussens, L.M., von Andrian, U.H., van Rheenen, J., Deryugina, E., and Friedl, P. (2009). Collagen-based cell migration models in vitro and in vivo. Semin. Cell Dev. Biol. *20*, 931–941.

Yasuda, K., Zhang, H., Loiselle, D., Haystead, T., Macara, I.G., and Mili, S. (2013). The RNA-binding protein Fus directs translation of localized mRNAs in APC-RNP granules. J. Cell Biol. *203*, 737–746.

Zalfa, F., Achsel, T., and Bagni, C. (2006). mRNPs, polysomes or granules: FMRP in neuronal protein synthesis. Curr. Opin. Neurobiol. *16*, 265–269.

Zhang, Y., O'Connor, J.P., Siomi, M.C., Srinivasan, S., Dutra, A., Nussbaum, R.L., and Dreyfuss, G. (1995). The fragile X mental retardation syndrome protein interacts with novel homologs FXR1 and FXR2. EMBO J. *14*, 5358–5366.

Developmental Cell

Supplemental Information

Global Analysis of mRNA, Translation, and Protein Localization: Local Translation Is a Key Regulator of Cell Protrusions

Faraz K. Mardakheh, Angela Paul, Sandra Kümper, Amine Sadok, Hugh Paterson, Afshan Mccarthy, Yinyin Yuan, and Christopher J. Marshall

Supplementary Figures and Legends:

Fig. S1. RNA-seq analysis of intracellular mRNA distributions between protrusions and the cell-body, related to Figure 2. A: Schematic representation of RNA-seq based protrusion transcriptomics analysis. **B:** Protrusion and Cell-body localized mRNAs defined by RNA-seq overlap significantly with a previously published microarray based protrusion/cell-body mRNA localization study (Mili et al., 2008). Log2 of Protrusion/Cell-body FPKM ratios from two RNA-seq replicate experiments were plotted against each other. Protrusion (Green), and cell-body (red) localized mRNAs from Mili et al., are highlighted on the graph. P-values for protrusion and cell-body enrichments of Mili et al., mRNAs groups are shown on the graph.

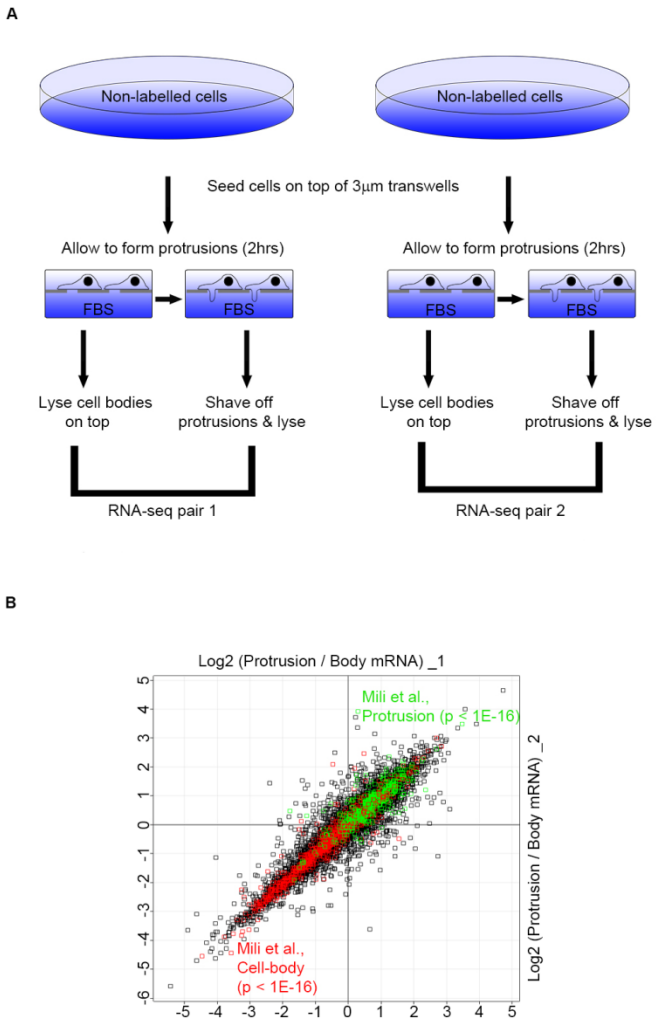

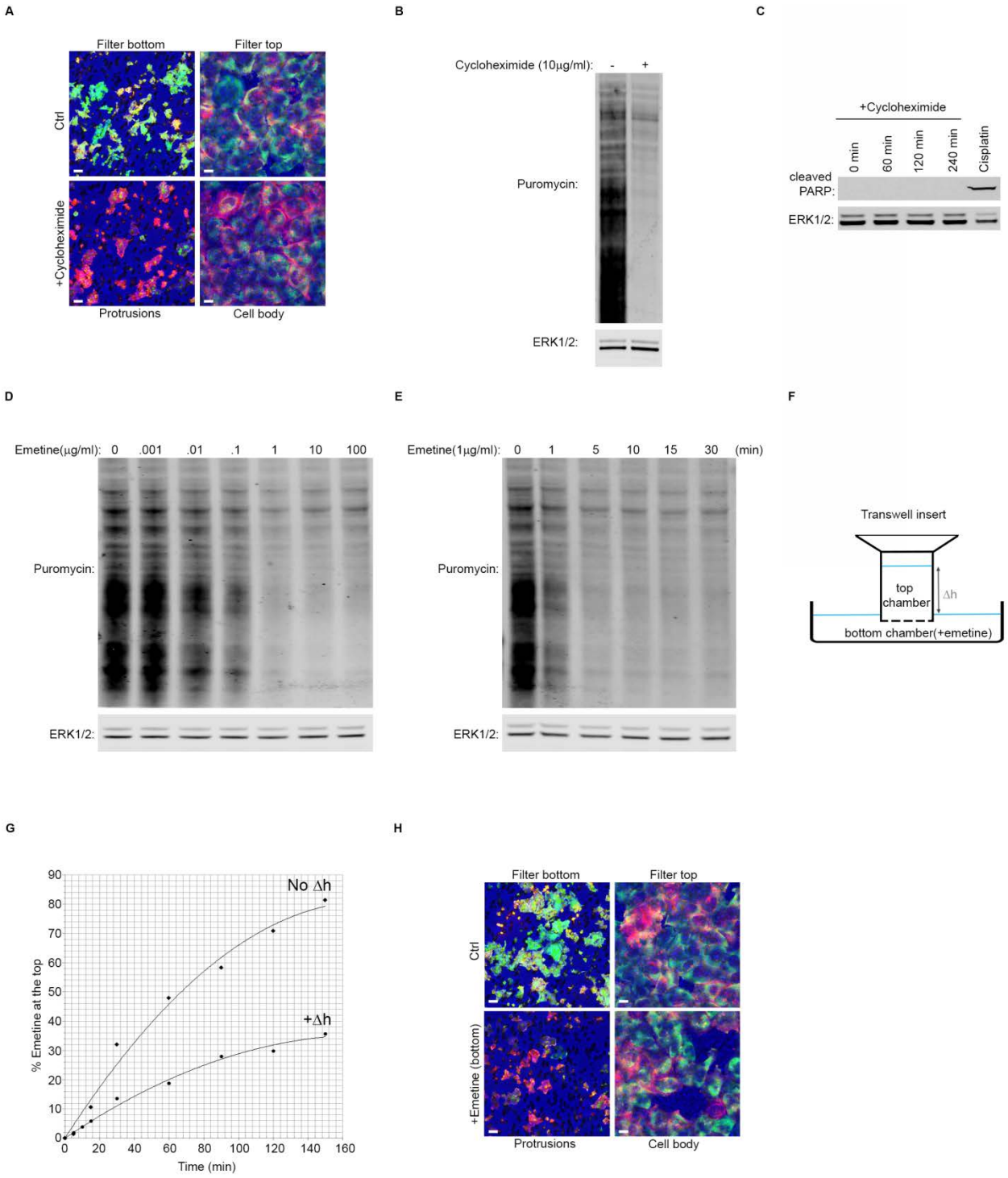

Fig. S2. Analysis of translation inhibition in MDA-MB231 cells, related to Figure 3. A: Protrusions are highly translationally active. MDA-MB231 mKate-CAAX (red) cells were seeded on collagen coated 3µm transwell filters and after 2hrs treated with or without 10µg/ml of

cycloheximide for 10 minutes, followed by puromycin treatment (10μg/ml) for 10 min to label nascent proteins. Afterwards, cells were fixed and visualized by immunofluorescence staining with an anti-puromycin antibody (green). Confocal images were taken from the top (right image) and bottom (left image) of the filter. The filter was visualized by transmitted light (blue). Scale bar = 10μm. Protrusions and the cell bodies show a strong puromycin staining which is abrogated upon cycloheximide treatment. **B:** Cycloheximide inhibition of protein translation in MDA-MB231 cells. MDA-MB231 cells were treated with 10μg/ml of cycloheximide for 10 minutes before being treated with puromycin (10μg/ml) for 10 min to label nascent proteins. Cells were then lysed and resolved by SDS-PAGE and blotted for puromycinylation, and ERK as loading control. **C:** Short-term treatment of MDA-MB231 cells with cycloheximide does not induce apoptosis. MDA-MB231 cells were treated with 10μg/ml of cycloheximide for indicated times before being lysed and analyzed by western blotting with a cleaved-PARP antibody as PARP cleavage marks apoptosis. Total ERK was used as loading control. Cisplatin treatment (20μg/ml for 24 hrs) was used as a positive control for apoptosis induction. **D:** Emetine dose response assessment of translation inhibition. MDA-MB231 cells were treated with indicated doses of emetine for 10 minutes before being washed and treated with puromycin (10μg/ml) to label nascent proteins. Cells were then lysed and resolved by SDS-PAGE and blotted for puromycinylation, and ERK as loading control. Emetine concentrations as low as 1μg/ml significantly inhibit protein translation. **E:** Emetine time-course of translation inhibition. MDA-MB231 cells were treated with 1μg/ml of emetine for indicated times before being washed and treated with puromycin (10μg/ml) to label nascent proteins. Cells were then lysed and resolved by SDS-PAGE and blotted for puromycinylation, and ERK as loading control. Emetine treatment times as short as 5 minutes significantly inhibit protein translation. **F:** Schematic representation

of emetine treatment setting for minimalizing bottom to top emetine diffusion. The level of liquid on top of the filter was kept significantly higher than that of the bottom where emetine was present, in order to create a positive hydrostatic pressure due to height difference (Δh). This slowly pushes the liquids from top to bottom through the transwell pores, thus slowing any upward diffusion from bottom to the top. **G:** Measurement of the diffusion of emetine from the bottom chamber to the top. Concentration of emetine at the top and the bottom of the filter was measured by reading its uv absorbance at 280nm. The amount of emetine on the top was then normalized to the initial amount measured from the bottom. Emetine exhibits a very slow diffusion from bottom to the top under the experimental settings of F, where a height difference (Δh) between the liquid levels is applied. **H:** Translation in protrusions can be specifically inhibited with a 5 minute Emetine treatment (1μg/ml) in the experimental setting of F, without affecting the cell-body translation. MDA-MB231 mKate-CAAX (red) cells were seeded on collagen coated 3μm transwell filters and after 2hrs, the bottom of the filter was treated with or without 1μg/ml of Emetine for 5 minutes as in F, followed by puromycin treatment (10μg/ml) for 10 min to label nascent proteins. Afterwards, cells were fixed and visualized by immunofluorescence staining with an anti-puromycin antibody (green). Confocal images were taken from the top (right image) and bottom (left image) of the filter. The filter was visualized by transmitted light (blue). Scale bar = 10μm. Puromycin staining is wiped out at the bottom of the filter while it is not significantly affected at the top.

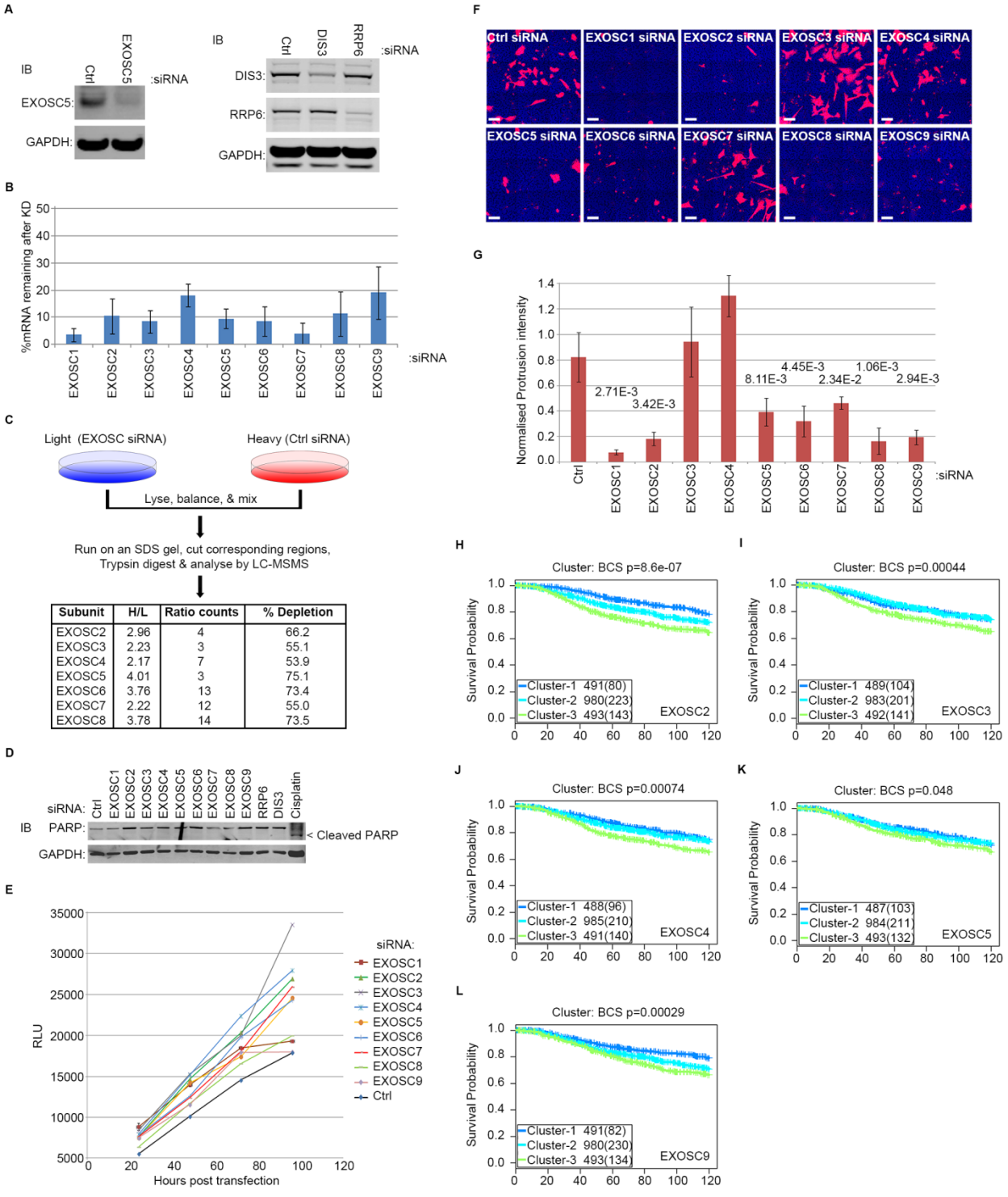

Fig. S3. Analysis of Exosome subunit depletion by siRNA, related to Figure 6. A: Test of exosome core and catalytic subunit antibody specificities. Left: Control and EXOSC5 depleted

MDA-MB231 cell lysates were run and blotted with anti-EXOSC5 antibody. EXOSC5 corresponding band is significantly reduced in EXOSC5 knockdown cells. Right: Control, RRP6, and DIS3 depleted MDA-MB231 cell lysates were run and blotted with anti-RRP6, and anti-DIS3 antibodies. RRP6 and DIS3 corresponding bands are significantly reduced in their respective knockdown cells. GAPDH was used as loading control. **B:** Quantitative PCR verification of siRNA mediated exosome core subunit knockdown at mRNA level in MDA-MB231 cells, 72hrs post-transfection. RNA contents for each exosome subunit knockdown were normalized to GAPDH RNA levels followed by ratio calculation to the non-targeting control values. All error bars are SD. **C:** SILAC based quantitative mass spectrometric verification of siRNA mediated exosome core subunit knockdowns at the protein level in MDA-MB231 cells, 72hrs post-transfection. Knockdown of each exosome core subunit was performed individually and in light SILAC labeled cells. After lysis, these knockdown lysates were then mixed with an equal amount of heavy SILAC labelled control siRNA knockdown lysates. ~10μg of each SILAC mix was then run on an SDS-PAGE gel, and the approximate region corresponding to the exosome subunits molecular weight was cut, trypsin digested, and analyzed by LC-MS/MS. Out of the total of 9 exosome core subunits, 7 were successfully identified and quantified. % of KD was then estimated from each calculated normalized H/L SILAC ratios. **D:** Short-term knockdown of exosome subunits does not induce apoptosis. MDA-MB231 cells were transfected with control vs. indicated siRNA of exosome core as well as RRP6 and DIS3 catalytic subunits. After 72hrs, the cells were lysed and analysed by western blotting for PARP cleavage which marks apoptosis. Cisplatin treatment (20μg/ml for 24 hrs) was used as a positive control. **E:** Short-term knockdown of exosome core subunits does not affect cell proliferation. MDA-MB231 cells were transfected with control siRNAs or siRNA against exosome core subunits. Viability

was then assessed at 24, 48, 72, and 96 hrs post transfection by CellTiter-Glo. All cells show linear and comparable growth rates apart from EXOSC1 and EXOSC9 which show a decrease but only at 96hrs post transfection. RLU: Random Luminescence Unit. **F:** Exosome core depletion inhibits protrusions in HT1080 cells. HT1080 Fibrosarcoma cells were transfected with control or exosome core subunit siRNAs. After 72hrs, the cells were seeded on collagen coated 3μm transwell filters to form protrusions before being fixed 4hrs later and analyzed by confocal microscopy. Cells were stained 24hrs prior to seeding by CellTracker-CMRA (red). Filter was visualized by transmitted light (blue). Scale bar = 50μm. The images show protrusions at the bottom of the filter. **G:** Quantification of protrusions from F (n = 4). All error bars are SD. **H:** Increased expression of exosome core subunit EXOSC2 correlates with bad prognosis in breast cancers. Kaplan-Meier plot of disease-specific survival (truncated at 10 years) for stratification by EXOSC2 gene expression in 1,980 breast cancer patients (Curtis et al., 2012). The dataset was divided into 3 clusters. Cluster-1 had the 25% lowest expression (blue). Cluster-3 had the 25% highest expression (green), and cluster-2 had the expression levels in between (cyan). For each cluster, the number of samples at risk is indicated as well as the total number of deaths (in parentheses). **I:** Increased expression of exosome core subunit EXOSC3 correlates with bad prognosis in breast cancers. Kaplan-Meier plot of disease-specific survival (truncated at 10 years) for stratification by EXOSC3 gene expression in 1,980 breast cancer patients as in H. **J:** Increased expression of exosome core subunit EXOSC4 correlates with bad prognosis in breast cancers. Kaplan-Meier plot of disease-specific survival (truncated at 10 years) for stratification by EXOSC4 gene expression in 1,980 breast cancer patients as in H. **K:** Increased expression of exosome core subunit EXOSC5 correlates with bad prognosis in breast cancers. Kaplan-Meier plot of disease-specific survival (truncated at 10 years) for stratification by EXOSC5 gene

expression in 1,980 breast cancer patients as in H. **L:** Increased expression of exosome core subunit EXOSC9 correlates with bad prognosis in breast cancers. Kaplan-Meier plot of disease-specific survival (truncated at 10 years) for stratification by EXOSC9 gene expression in 1,980 breast cancer patients as in H.

Supplemental Data Files, and Movie Legends:

Supplemental Data File 1: Proteomics, transcriptomics, and local translation rate analysis datasets, related to Figure 2. **A:** SILAC protein ratios between protrusion and cell-body fractions from two reciprocally labelled experiments. **B:** Perseus output for 1D annotation enrichment analysis of protein distributions from 1A (Benjamini-Hochberg FDR = 0.02). Actin cytoskeleton related categories are marked in blue; RNA binding/Ribosomal protein categories are marked in green. **C:** RNA-seq FPKM ratios between protrusion and cell-body fractions from two replicate experiments**. D:** Pulsed SILAC (H/M) ratios between protrusion and cell-body fractions from two reciprocally pulse-labelled experiments **E:** Perseus output for 2D annotation enrichment analysis of Protein versus translation rate distributions between protrusions and the cell-body (Benjamini-Hochberg FDR = 0.02). Actin cytoskeleton related categories are marked in blue; RNA binding/Ribosomal protein categories are marked in green; all organelle related protein categories are marked in red.

Supplemental Data File 2: Category enrichment and UTR element analyses, related to Figure 4: A: Perseus output for 2D annotation enrichment analysis of mRNA versus translation rate distributions between protrusions and the cell-body (Benjamini-Hochberg FDR = 0.02). Actin cytoskeleton related categories are marked in blue; RNA binding/Ribosomal protein categories are marked in green; Mitochondrial related protein categories are marked in purple; all other organelle related protein categories are marked in red. **B:** List of all UTR elements investigated in Figure 4C (Source: UTRscan (Grillo et al., 2010)).

Movie S1: (related to Figure 1) Protrusions initiate and grow stably through 3μm transwell filter pores. MDA-MB231 mKate CAAX cells were seeded on collagen coated 3μm transwell filters and time-lapsed for 5hrs at 5 minute intervals as they formed protrusions through the pores. Red: Cell membranes, Blue: filter. Left image shows protrusions at the bottom of the filter. Right image shows cell-bodies at the top of the filter. Scale bar = 10μm

Movie S2: (related to Figure 1) Protrusions initiate and grow stably through pores of 3D collagen-I matrix. MDA-MB231 cells were seeded on 3D pepsinised collagen-I gels and time-lapsed for 5-10 hrs at 3 minute intervals as they formed protrusions. Arrow marks a protrusion that remains stable through the course of imaging. Scale bar = 10μm

Movie S3: (related to Figure 3) Protrusions initiate but are not stable and retract back in Cycloheximide (CHX) treated cells. MDA-MB231 mKate CAAX cells were seeded on collagen coated 3μm transwell filters and time-lapsed for 4hrs at 15 minute intervals as they

formed protrusions through the pores of transwell filters in the presence (right) or absence (left) of 10μg/ml CHX. Red: Cell membranes, Blue: filter. Scale bar = 20μm. The images show protrusions at the bottom of the filter.

Movie S4: (related to Figure 3) Protrusions initiate but are not stable and retract back in Cycloheximide (CHX) treated cells in 3D collagen. MDA-MB231 cells were seeded on 3D pepsinised collagen-I gels and time-lapsed for 10 hrs at 3 minute intervals as they formed protrusions in the presence (right) or absence (left) of 10μg/ml CHX. Scale bar = 10μm.

Movie S5: (related to Figure 3) Protrusions are destabilized upon inhibition of local translation by local emetine treatment. MDA-MB231 mKate CAAX cells were seeded on collagen coated 3μm transwell filters for 2 hrs before being treated with 1μg/ml emetine (right) or mock treated (left) for 5 minutes as in Fig. S2F. After the treatment, the cells were time-lapsed for 2hrs at 5 minute intervals to capture protrusion dynamics. Red: Cell membranes, Blue: filter. Scale bar = 20μm. The images show protrusions at the bottom of the filter.

Movie S6: (related to Figure 6) Protrusions initiate but are not stable and retract back in exosome core depleted MDA-MB231 cells. Control (left) or EXOSC5 depleted (right) MDA-MB231 mKate CAAX cells were seeded on collagen coated 3μm transwell filters and time-lapsed for 4hrs at 30 minute intervals as they formed protrusions through the pores of transwell filters. Red: Cell membranes, Blue: filter. Scale bar = 20μm. The images show protrusions at the bottom of the filter.

Movie S7: (related to Figure 6) Protrusions initiate but are not stable and retract back in exosome core depleted MDA-MB231 cells in 3D collagen. Control (left) or EXOSC5 depleted (right) MDA-MB231 cells were seeded on 3D pepsinised collagen-I gels and time-lapsed for 10 hrs at 3 minute intervals as they formed protrusions. Scale bar = 10μm.

Supplemental Experimental Procedures:

Antibodies, reagents, and plasmids:

Rabbit monoclonal antibodies against ERK1/2 (137F5), VASP (3132), H2AX (7631), PARP (46D11), and cleaved PARP (D64E10), were all from Cell Signaling Technology. Mouse monoclonal anti-GAPDH antibody was from Novus Biologicals. Mouse monoclonal anti-puromycin (12D10) was from Millipore. Rabbit polyclonal anti-EXOSC5 antibody was a gift from Ger Pruijn (Department of Biomolecular Chemistry, Radboud University Nijmegen, Nijmegen, The Netherlands). Mouse monoclonal and rabbit polyclonal antibodies against DIS3 and RRP6 were from Abcam. Hoechst 33258 pentahydrate, CellTracker-CMFDA, CellTracker-CMRA, CellTrace Far Red DDAO-SE, and Alexa Fluor-488 Phalloidin were from Life Technologies Molecular Probes. All secondary antibodies were also from Life Technologies Molecular Probes. Cycloheximide and Emetine dihydrochloride hydrate were from Sigma-Aldrich. All siRNAs (siGENOME Smartpool) were purchased from Dharmacon. Quantitative-PCR probes were purchased from Primer Design and Qiagen. Polycarbonate transwell filters were from Corning. Bovine Collagen (PureCol, 3mg/ml) was from Advanced BioMatrix. CellTiter-Glo was purchased from Promega. Membrane targeted mKate (pmKate2-f-mem) expression construct was purchased from Evrogen.

Cell staining, Immunofluorescence, and confocal microscopy

Staining with CellTracker dyes was performed according to manufacturer's instructions 24 hrs prior to analysis. CellTracker-CMFDA was used at 1.25μM, and CellTracker-CMRA at 5μM. CellTrace Far Red DDAO-SE staining of collagen coated filters was also done 24hrs prior to

analysis. Filters were stained with 100μM dye in PBS for 20 minutes followed by 3 PBS washes and kept in PBS at 4°C in darkness before seeding of the cells. For immunofluorescence staining on coated cover slips or transwells, cells were seeded and fixed after 2hrs (or as indicated otherwise) with PBS / 4%Formaldehyde, permeabilised by PBS / 0.2% Triton, and blocked in PBS / 4%BSA for 20 minutes before being incubated with primary and secondary antibodies (1:200) for one hour in blocking buffer. 3 x PBS washes were performed in between each antibody step. Phalloidin (1:100) and Hoechst (1:5000) staining was also done in blocking buffer for 20 minutes. Time-lapse analysis on protrusions in 3D collagen was performed on a Nikon Eclipse TE2000-S inverted epi-fluorescence microscope with a Hamamatsu cooled CCD camera using a 20x NA objective. Immunofluorescence and transwell imaging were performed on a Ziess LSM 710 confocal microscope with a 63x NA oil objective at optimal aperture settings. 4 times averaging per image was used. For time-lapse confocal analysis, the filter was placed on a glass bottomed 35mm dish containing DMEM with 10% serum right after seeding, and imaged in a live imaging chamber (37°C/10%CO_2) by confocal microscopy for indicated times. A tile scan of 3x3 contiguous fields of view was taken at 2 Z-planes (top and bottom of the filter) as before. In both fixed and live conditions, the filter was either visualized by collagen staining with CellTrace Far Red DDAO-SE, or by confocal transmitted light imaging.

3D collagen invasion, and 3D collagen morphology assays:

For 3D collagen invasion assay cells were suspended in serum-free collagen (2.3mg/ml) to a final concentration of 10,000cells/100μl. For each condition, 100μl aliquots were dispensed into 96-well ViewPlates (Perkin-Elmer) pre-coated with 0.2% fatty acid free BSA. 4 to 8 wells were used per condition. Plates were then centrifuged at 300g to collect the cells at the bottom of the

wells, and incubated at 37°C/10% CO2 for 3hrs to let the collagen set into a gel. 30µl DMEM with 10% serum was then added to the top and cells were left to invade up through the collagen gel for 24hrs before being fixed and stained with Hoechst (5µg/ml). The plates were then imaged by an Operetta High Content Imaging System (PerkinElmer) using Z-planes at 0µm, 30µm, & 60µm. The invasion index was calculated as the number of cells at 30µm and 60 µm divided by the total number of cells. For 3D imaging of invaded cells, cells were stained by CellTracker-CMRA 24hrs prior to invasion assays. Following fixation, sequential Z-sections of the collagen embedded cells were obtained at 5µm intervals from 0µm to 105µm. For morphology analysis on 3D collagen (1.7mg/ml bovine pepsinised in DMEM), cells were seeded in 10% serum containing DMEM and allowed to adhere before treatment and imaging on a phase contrast microscope using the 10x objective (Nikon).

RNAi screening of RNA Binding Domain (RBD) containing proteins

For RNAi screening of RBD containing proteins, 10,000 cells were seeded on top of collagen coated 96-well HTS transwell filters (3µm pore) without media in the bottom chamber, and transfected the next day with the siRNA library (10nM). After 72hrs, media on the cells was replaced with 70µl serum-free DMEM and 200µl DMEM with 10% serum was added to the bottom chamber of each well to start protrusion formation. After 4hrs, cells were fixed and imaged by confocal microscopy. Four 3x3 tile scans from two wells per each siRNA were used.

Mass spectrometry sample preparation and LC-MS/MS analysis

For in-gel digestion, excised gel sections were diced and reduced with 5 mM TCEP, alkylated with 55 mM iodoacetamide, and trypsin digested with modified porcine Trypsin (Promega) at

37°C overnight. After digestion, peptides were extracted with acetonitrile and triethylammonium bicarbonate washes. The solution was dried in a speedvac, and reconstituted in 2% acetonitrile/0.1% formic acid for LC-MS/MS. LC-MS/MS runs were performed by ICR's proteomics core facility. Briefly, 40% of each fraction was analysed as 4µL injections using HP1200 reversed phase chromatography platform (Agilent). Peptides were resolved on a 75 µm I.D. C18 Pepmap column with 3 µm particle size (LC Packings/Dionex) over 90 min using a linear gradient of 96:4 to 50:50 buffer A:B (buffer A: 2% acetonitrile/0.1% formic acid; buffer B: 80% acetonitrile/0.1% formic acid) at 300nL/min. Peptides were ionized by electrospray ionization using 1.9 kV applied directly to the post-column LC eluent via a microtee built into the nanospray source. Sample was infused into an LTQ Velos Orbitrap mass spectrometer (Thermo Fisher Scientific) using a 20 µm I.D., 10 µm tapered tip non-coated SilicaTip emitter (New Objectives). The ion transfer tube was heated to 200°C and the S-lens set to 60%. MS/MS were acquired using data dependent acquisition to sequence the top 20 most intense ions using standard ion trap scans. Automatic gain control was set to 1,000,000 for FT-MS and 30,000 for IT-MS/MS, full FT-MS maximum inject time was 500ms and normalized collision energy was set to 35% with an activation time of 10ms. Wideband activation was used to co-fragment precursor ions undergoing neutral loss of up to -20 m/z from the parent ion, including loss of water/ammonia. MS/MS was acquired for selected precursor ions with a single repeat count followed by dynamic exclusion with a 10ppm mass window for 15s based on a maximal exclusion list of 500 entries.

Proteomics search and SILAC quantifications

All mass spectrometry raw files were searched and quantified by Maxquant software (Cox and Mann, 2008; Cox et al., 2011). The search was performed using the Andromeda search engine, against the Human IPI database (version 3.68). Mass tolerance filters of 6ppm and 0.5Da were used for precursor and fragment masses, respectively. A minimum peptide length of 6 amino acids was used. Second-peptide search, and match between runs (2 minutes window) option, were all enabled. For total SILAC, but not the pulsed-SILAC (pSILAC) analysis, the re-quantify option was also enabled. Methionine oxidation and N-terminal acetylation were added as variable modifications while carbamidomethylation was considered as a fixed modification on Cysteine. A maximum of 2 missed cleavages were allowed, and the false discovery rate (FDR) was set at 0.01 for both peptide and protein identifications. For total SILAC quantifications, an overall minimum ratio count (H/L) of 2 per protein was used. For pSILAC, this was set to 1 (H/M). Only razor or unique unmodified peptides as well as Methionine oxidized and N-terminally acetylated peptides were used for protein quantifications. Data analysis on the search results was performed by Perseus software (Cox and Mann, 2012), using the Maxquant 'protein groups' output file as input. The median subtracted normalized ratios were used for all downstream data analyses.

RNA-seq sample prep, sequencing, and analysis

Sample prep and Illumina sequencing were performed by ICR's tumor profiling unit. Briefly, total RNA quality was assessed using the 2100 Bioanalyzer (Agilent). Poly-A mRNA was then isolated from the total RNA sample using the Dynabeads mRNA Purification Kit (Life Technologies). Purified mRNAs were fragmented using the mRNA Fragmentation Reagents (Life Technologies) and ethanol precipitated. The size range of generated fragments was kept at

60 to 1000 nucleotides, with a peak at around 150 nucleotides. To make cDNA from the fragmented RNA samples, NEBNext mRNA Library Prep Reagent Set for Illumina was used (NEB), with the synthesis being performed Strand-wise (first-strand synthesis then second-strand synthesis) followed by purification using QIAquick Columns (Qiagen). End Repair, dA-tailing, and Adapter ligation were all performed based on NEBNext mRNA Library Prep Reagent Set for Illumina instructions. Agarose gel separation was used to select for the appropriate library size. To get a library size of ≈400bp (insert size ≈330bp) a 350-500bp slice was taken from each of the samples. Gel extraction was then performed using Qiagen MinElute gel extraction kit (Qiagen). To enrich for the correctly adapter-ligated and size-selected cDNA, a PCR was performed using the Herculase II polymerase enzyme (Agilent), also adding the specific indexes for multiplexing. The PCR was then followed by an AMPure bead purification to exclude primer-dimers and other smaller fragments from the final library. The quantity and quality of the prepared library was evaluated on Bioanalyzer and the samples were quantified using qPCR. Subsequently, libraries were combined for multiplexed sequencing runs. For sequencing Read-1 and Read-2, the sequencing primers provided with the PE Cluster Generation kits were used. RNA-seq data was acquired on a HiSeq2000 (Illumina) sequencer, generating 2 x 76 bp reads. Sequences were then processed by ICR's tumor profiling unit (FASTQ file creation, de-multiplexing, filtering failed reads, and Tophat analysis) and a single tab-delimited list of mRNAs with their corresponding Fragment Per Kilo-base per Million (FPKM) values was generated. Hits with FPKM values less than 1 were filtered out. Any non-coding sequences were also filtered out. Protrusion to cell-body FPKM ratios were calculated for each biological replicate. All downstream data analysis was then performed using Perseus (Cox and Mann, 2012).

Graphs, bioinformatics, and statistical analysis

All proteomics and RNA-seq graphs were generated by Perseus (Cox and Mann, 2012). All Bioinformatics analyses of proteomics and RNA-seq datasets were also performed by Perseus. The annotation enrichment analysis was performed using 1D or 2D annotation enrichment algorithms. A Benjamini–Hochberg false discovery rate (FDR) of 0.02 was used to correct for annotation enrichment p-values. For UTR analysis, the data was annotated for different UTR elements using UTRref database and UTRscan tool (Grillo et al., 2010). Pearson correlation coefficients and p-values for correlations were also generated with Perseus. All bar graph were generated by Microsoft Excel. For protrusion, morphology, and migration assays, P-values were calculated against control populations using two-tailed, heteroscedastic t-test analysis. All error bars are standard deviation (SD).

References

Cox, J., and Mann, M. (2008). MaxQuant enables high peptide identification rates, individualized p.p.b.-range mass accuracies and proteome-wide protein quantification. Nat Biotechnol *26*, 1367-1372.

Cox, J., and Mann, M. (2012). 1D and 2D annotation enrichment: a statistical method integrating quantitative proteomics with complementary high-throughput data. BMC Bioinformatics *13 Suppl 16*, S12.

Cox, J., Neuhauser, N., Michalski, A., Scheltema, R.A., Olsen, J.V., and Mann, M. (2011). Andromeda: a peptide search engine integrated into the MaxQuant environment. J Proteome Res *10*, 1794-1805.

Curtis, C., Shah, S.P., Chin, S.F., Turashvili, G., Rueda, O.M., Dunning, M.J., Speed, D., Lynch, A.G., Samarajiwa, S., Yuan, Y., *et al.* (2012). The genomic and transcriptomic architecture of 2,000 breast tumours reveals novel subgroups. Nature *486*, 346-352.

Grillo, G., Turi, A., Licciulli, F., Mignone, F., Liuni, S., Banfi, S., Gennarino, V.A., Horner, D.S., Pavesi, G., Picardi, E., *et al.* (2010). UTRdb and UTRsite (RELEASE 2010): a collection of sequences and regulatory motifs of the untranslated regions of eukaryotic mRNAs. Nucleic acids research *38*, D75-80.

Mili, S., Moissoglu, K., and Macara, I.G. (2008). Genome-wide screen reveals APC-associated RNAs enriched in cell protrusions. Nature *453*, 115-119.